SUPPLEMENTARY INFORMATION

Annotating MYC oncogene status with ^{89}Zr-transferrin imaging

Jason P. Holland,[1,Δ]† Michael J. Evans,[2]† Samuel L. Rice,[1] John Wongvipat,[2]

Charles L. Sawyers[2,3]* and Jason S. Lewis[1,4]*

† JPH and MJE contributed equally to this work

[1] Radiochemistry Service, Department of Radiology, Memorial Sloan-Kettering Cancer Center, 1275 York Avenue, New York, U.S.A., NY10065.

[2] Human Oncology and Pathogenesis Program, Memorial Sloan-Kettering Cancer Center, 1275 York Avenue, New York, U.S.A., NY10065.

[3] Howard Hughes Medical Institute.

[4] Program in Molecular Pharmacology and Chemistry, Memorial Sloan-Kettering Cancer Center, 1275 York Avenue, New York, U.S.A., NY10065.

[Δ] Present address: Division of Nuclear Medicine and Molecular Imaging, Massachusetts General Hospital, Harvard Medical School, 55 Fruit St., White 427, Boston, Massachusetts, U.S.A. MA02114.

*** Corresponding Authors:**

Jason S. Lewis, Ph.D.
Radiochemistry Service
Department of Radiology
Memorial Sloan-Kettering Cancer Center
1275 York Avenue, New York, NY10065

Tel: 16468883038
Fax: 16464220408
E-mail: lewisj2@mskcc.org

Charles L. Sawyers, M.D.
Howard Hughes Medical Institute
Human Oncology and Pathogenesis Program
Memorial Sloan-Kettering Cancer Center
1275 York Avenue, New York, NY10065

Tel: 16468882594
Fax: 16468882595
E-mail: sawyersc@mskcc.org

Table of Contents

Methods and Materials

General details

All chemicals, unless otherwise stated, were purchased from SigmaAldrich (St. Louis, MO) and were used as received. Water (>18.2 MΩ·cm at 25 ºC, Milli-Q, Millipore, Billerica, MA) was purified by passing through a 10 cm column of chelex resin (Bio-Rad Laboratories, Hercules, CA) at a flow rate <1.0 mL/min. All instruments were calibrated and maintained in accordance with previously reported routine quality-control procedures[1]. Radioactivity was measured by using a Capintec CRC-15R Dose Calibrator (Capintec, Ramsey, NJ) with a calibration factor of 465 for ^{89}Zr. For accurate quantification of radioactivity, experimental samples were counted for 1 min. on a calibrated Perkin Elmer (Waltham, MA) Automatic Wizard[2] Gamma Counter using a dynamic energy window of 800–1000 keV for ^{89}Zr (909 keV emission). Appropriate decay correction was employed throughout. ^{89}Zr-radiolabeling reactions were monitored by using silica-gel impregnated glass-fibre instant thin-layer chromatography (ITLC-SG) paper (Pall Corp., East Hills, NY) and analyzed on a radio-TLC plate reader (Bioscan System 200 Imaging Scanner coupled to a Bioscan Autochanger 1000 (Bioscan Inc., Washington, DC, using Win-Scan Radio-TLC software version 2.2). Solvent systems included diethylene triamine pentaacetic acid in water (DTPA, 50 mM, pH7) and phosphate buffered saline (PBS).

Protein conjugation

Mouse apo-transferrin (SigmaAldrich, St. Louis, MO), human apo-transferrin (SigmaAldrich) and mouse serum albumin (SigmaAldrich) were conjugated to desferrioxamine B (DFO; Calbiochem, Spring Valley, CA) and radiolabelled with ^{89}Zr-oxalate to give ^{89}Zr-mTf, ^{89}Zr-hTf and ^{89}Zr-mAlb, respectively, using procedures derived from previous studies on radiolabelled monoclonal antibodies for immuno-PET (Supplementary Fig. 1)[2].

Supplementary Figure 1. Schematic of the protein conjugation and ^{89}Zr-DFO labelling strategy

Protein crystal structure adapted from Protein Data Bank (PDB) ID: 1a8e[3].

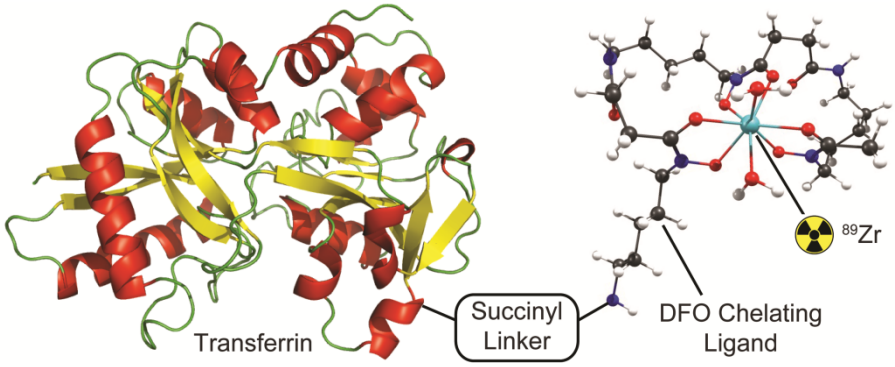

Synthesis of N-succinyldesferrioxamine B (N-succDFO). DFO mesylate (0.508 g, 0.77 mmol, Calbiochem, Spring Valley, CA) was dissolved in pyridine (7.5 mL) and reacted with excess succinic anhydride (1.704 g, 0.017 mol) at room temperature for 24 h. The white suspension was then poured into NaOH(aq.) (120 mL, 0.015 mol dm^{-3}) and stirred at room temperature for 16 h. The colorless solution was adjusting to pH2 by the addition of HCl (12 mol dm^{-3}) aliquots and cooled with stirring at 4 ºC for 2 h. The white precipitate was collected by filtration, washed with copious amounts of HCl (0.01 mol dm^{-3}) then water and dried *in vacuo* to give the *N*-succinyldesferrioxamine B (*N*-succDFO) as a white, microcrystalline solid (0.306 g, 4.75×10^{-4} mol, 62%). HRMS-ES$^+$: Calc. for [$C_{29}H_{52}N_6O_{11}$ + H^+] = 661.3772; found 661.3760 ([M + H^+] = 100%).

Preparation of [Fe(N-succDFO-TFP)] activated ester. *N*-succDFO (9.0 mg, 14 µmol) was suspended in 3.0 mL sterile saline and the pH adjusted to 6.5 with 0.1 M Na_2CO_3(aq.) (50 – 75 µL in chelex purified water). Then a solution of $FeCl_3$•$6H_2O$ [4.0 mg, 15 µmol, 300 µL of 0.1 M HCl(aq.)] was added. Upon addition of the $FeCl_3$(aq.) the reaction mixture changes from colourless to deep orange due to the intense electronic absorption band of [Fe(DFO)] with a peak at 430 nm (ε_{430} = 2216 ± 49 mol^{-1} dm^3 cm^{-1}). After stirring the reaction at room temperature for 1

h, a solution of 2,3,5,6-tetrafluorophenol (TFP, 300 μL, 36 μmol, 1.2 mol dm^{-3} in chelex purified MeCN; SigmaAldrich, St. Louis, MO) was added to the reaction followed by addition of solid *N*-(3-dimethylaminopropyl)-*N'*-ethylcarbodiimide hydrochloride (EDAC, 120 mg, 0.63 mmol, SigmaAldrich). The reaction mixture (pH6.5) was then stirred at room temperature for 1 h before purifying the [Fe(*N*-succDFO-TFP)] product by use of a C-18 Light Sep-pak cartridge (Waters, Milford, MA). The reaction mixture was loaded onto a pre-activated (6 mL MeCN, 10 mL H_2O) C-18 cartridge, washed with copious amounts of water (>40 mL), and eluted with 1.5 mL MeCN. The final [Fe(*N*-succDFO-TFP)] solution had a maximal concentration of approximately 9.8 mM. NB: The [Fe(*N*-succDFO-TFP)] solution can be stored for at least 14 days at 4 ºC but the most efficient conjugation reactions were achieved by using fresh preparations.

DFO conjugation to proteins To 3 separate centrifuge vials was added mouse apo-transferrin (3 mg/mL, 1 mL, 38 nmol, MW 76–81 kDa), human apo-transferrin (5 mg/mL, 1 mL, 64 nmol, MW 76–81 kDa), and mouse serum albumin (5 mg/mL, 1 mL, 72 nmol, MW 69 kDa), and the pH adjusted to 9.5 – 10.0 by using aliquots of 1.0 M and 0.1 M Na_2CO_3(aq.). Then 4 equivalents of [Fe(*N*-succDFO-TFP)] was added and the solutions mixed gently using an automated pipette. Reactions were allowed to proceed at room temperature for 1 h before the pH was adjusted to 3.9 – 4.2 by addition of <10 μL aliquots of 0.25 M H_2SO_4(aq.). Then a 10-fold excess of ethylenediaminetetraacetic acid disodium salt ($EDTA^{2-}.2Na^{+}$(aq.), 0.0674 mol dm^{-3} in chelex 100 resin treated deionised water) with respect to [Fe(*N*-succDFO-TFP)] was added. The reactions were incubated in a water bath at 38 ºC for 1 h during which time the solutions changed from clear yellow to colourless. The DFO-conjugated mouse apo-transferrin (mTf), DFO-human apo-transferrin (hTf) and DFO-mouse serum albumin (mAlb) were purified by size-exclusion chromatography (Sephadex G-25 M, PD-10 column, >30 kDa, GE Healthcare; dead-volume = 2.5 mL, eluted with 200 μL fractions of sterile saline to a total volume of 1.8 mL of isolated protein).

Radiolabelling

Zirconium-89 was produced *via* the $^{89}Y(p,n)^{89}Zr$ transmutation reaction on an EBCO TR19/9 variable beam energy cyclotron (Ebco Industries Inc., Richmond, British Columbia, Canada) in accordance with previously reported methods[4]. The ^{89}Zr-oxalate was isolated in high radionuclidic and radiochemical purity (RCP) >99.9%, with an effective specific-activity of 195–497 MBq/μg, (5.28–13.43 mCi/μg).

^{89}Zr-mTf, ^{89}Zr-hTf and ^{89}Zr-mAlb were prepared by the complexation of ^{89}Zr-oxalate with DFO-conjugated mTf, hTf and mAlb, respectively. Typical radiolabelling reactions were conducted in accordance with previously reported methods[2] used for labelling monoclonal antibodies with ^{89}Zr. As an example, typical conditions used to produce ^{89}Zr-mTf are presented. The same methods were used to produce ^{89}Zr-hTf and ^{89}Zr-mAlb. Briefly, ^{89}Zr-oxalate (380 MBq, [10.26 mCi]) in 1.0 M oxalic acid (250 μL) was adjusted to pH7.7–8.1 with 1.0 M Na_2CO_3(aq.). CAUTION: Acid neutralization releases CO_2(g) and care should be taken to ensure that no radioactivity escapes the microcentrifuge vial. After CO_2 evolution ceased, DFO-conjugated mTf (700 μL, 1.36 mg/mL [0.95 mg of protein], in sterile saline) was added and the reaction was mixed gently by aspirating with a pipette. The reaction was incubated at room temperature for between 1–2 h and complexation progress was monitored with respect to time by ITLC (DTPA, 50 mM, pH7). After 1 h, crude radiolabelling yields and RCP were typically >95%. ^{89}Zr-mTf was purified by using spin-column centrifugation (4 mL total volume, >30 kDa particle retention, Amicon Ultra-4, Millipore, Billerica, MA; washed with 4×3 mL sterile saline). The radiochemical purity (RCP) of the final ^{89}Zr-mTf (formulation: pH5.5–6.0; <500 μL; sterile saline) was measured by both radio-ITLC and analytical size-exclusion chromatography (PD-10 column; loading <0.55 MBq [<15 μCi], ca. 5–10 μL aliquots; eluted with 50×0.2 mL saline fractions). In the ITLC experiment the ^{89}Zr-mTf, ^{89}Zr-hTf, ^{89}Zr-mAlb and ^{89}Zr-DFO remain at the baseline (R_f = 0.0), whereas $^{89}Zr^{4+}$(aq.) ions and the complex ^{89}Zr-DTPA elute with the solvent front (R_f = 1.0). The final radiochemical yield of the purified ^{89}Zr-mTf was typically >80% and the product was formulated in sterile saline with RCP >99% (n = 7) and a specific-activity of 331.4±12.2 MBq/mg (8.96±0.32 mCi/mg) of protein. The specific-activity of the purified and formulated ^{89}Zr-hTf was 215.8±5.5 MBq/mg (5.83±0.15 mCi/mg) of protein (n = 3), and for ^{89}Zr-mAlb was 160.2±4.6 MBq/mg (4.33±0.12 mCi/mg; n = 4) of protein.

Supplementary Figure 2 shows typical radio-ITLC chromatograms of the crude and purified ^{89}Zr-mTf and Supplementary Figure 3 shows a typical elution profile for the purification of ^{89}Zr-mTf by using PD-10 size-exclusion chromatography (*vide infra)*.

Chelate number

The number of accessible DFO chelates conjugated to mTf, hTf and mAlb was measured by radiometric isotopic dilution assays following a method similar to that described previously[2,5,6]. From a stock solution, aliquots of ^{89}Zr-oxalate (5 μL, 370 kBq [10 μCi], pH7.7-7.9 [pH adjusted using 1.0 M Na_2CO_3]) were added to 12 solutions containing 1:2 serial dilutions of non-radioactive $ZrCl_4$(aq.) (50 μL fractions; 1000–0.5 pmol, pH7.7). The mixture was vortexed for 30 s before adding 5 μL aliquots of mTf (1.36 mg/mL, 6.8 μg of mAb, 0.087 nmol; sterile saline), hTf (2.20 mg/mL, 11.0 μg of mAb, 0.14 nmol, in saline), or mAlb (2.15 mg/mL, 10.8 μg of mAb, 0.16 nmol; sterile saline). The reactions were incubated at room temperature for >2 h before quenching with DTPA (20 μL, 50 mM, pH7.0). Control experiments confirmed that ^{89}Zr complexation to DFO-conjugated proteins was complete in <2 h. The extent of complexation was assessed by developing ITLC strips (DTPA, 50 mM) and counting the activity at the baseline and solvent front. The fraction of ^{89}Zr-radiolabelled protein (A_b) was plotted *versus* the amount of non-radioactive $ZrCl_4$ added. The number of chelates was calculated by measuring the concentration of $ZrCl_4$ at which only 50% of the protein was labelled, multiplying by a factor of 2, and then dividing by the moles of protein present in the reaction. Isotopic dilution assays revealed an average of 1.9±0.2, 1.7±0.3 and 2.1±0.3 accessible chelates per protein molecule for mTf, hTf and mAlb, respectively.

Stability studies

The stability of ^{89}Zr-mTf, ^{89}Zr-hTf and ^{89}Zr-mAlb with respect to change in radiochemical purity and loss of radioactivity from the protein fraction was investigated *in vitro* by incubation in solutions of saline, and PBS for 5 days at 37 ºC. RCP was determined by radio-ITLC and γ-counting, and the protein-labelled fraction was measured at various time points by size-exclusion chromatography (PD-10, Sephadex G-25M, GE Healthcare). In all cases, ^{89}Zr-mTf, ^{89}Zr-hTf and

^{89}Zr-mAlb were found to be stable with respect to change in RCP and loss of the radionuclide from the protein with <1% loss of ^{89}Zr over 5 days incubation under various conditions (see **Supplementary Table S1** below). These results are consistent with previous observations on ^{89}Zr-radiolabelled monoclonal antibodies and affirm the use of DFO as a chelate for ^{89}Zr radiotracer development[2,7].

***In vitro* and *in vivo* metabolism studies by HPLC**

In addition to the *in vitro* stability studies described above, the stability of the ^{89}Zr-mTf and ^{89}Zr-hTf radiotracers with respect to change in RCP due to aggregation, transmetallation or catabolic degradation of the complexes was assessed *in vitro* and *in vivo* by using size-exclusion, radiometric, high-performance liquid chromatography (radio-HPLC). The radio-HPLC system was equipped with a Tosoh Science G3000SWXL column (300 mm × 7.8 mm; 5 μm; Fisher Scientific, Pittsburgh, PA), and eluted with a 0.02 M sodium acetate, 0.15 M sodium chloride, pH6.4 mobile phase at flow rate of 1 mL/min. at ambient temperature. Fractions (30 × 1 mL samples) were collected and counted for ^{89}Zr-radioactivity using a calibrated gamma counter. For analysis, counts-per-minute (CPM) data were background and decay corrected, and the cumulative (integrated) fraction of activity was plotted as a function of elution volume / mL.

For *in vitro* studies, formulated samples of ^{89}Zr-mTf(apo) (10.5 MBq, [285 μCi], 32 μg of protein) and ^{89}Zr-hTf(apo) (4.15 MBq, [112 μCi], 19 μg of protein), were incubated in saline (250 μL; control), or human blood (250 μL) for 24, 48 and 96 h, at 37 °C. For *in vivo* stability/metabolism studies, ^{89}Zr-mTf(apo) (Specific Activity = 331.4±12.2 MBq/mg [8.96±0.32 mCi/mg] of protein; injected dose = 10.5–11.5 MBq, [286–310 μCi], 32–35 μg of protein, in 200 μL sterile saline for injection) was injected i.v. in immunocompetent FVB male mice (t = 0 h; n = 6). At 24, 48 and 96 h post-radiotracer administration, blood and urine samples were collected (n = 2/time point) and analysed by radio-HPLC. Urine samples were injected onto the HPLC directly; for analysis of blood samples, cells were first remove by standard centrifugation then samples of plasma were injected onto the column. Both ^{89}Zr-mTf and ^{89}Zr-hTf were found to have a retention time of ~16 min., whereas small molecule metabolites eluted at ~22 min. and radioactive aggregates/transmetallated species (of unknown composition) had a shorter retention time <16 min.

In vitro cellular uptake studies

MycCaP[8] and HeLa (ATCC, Manassas, VA) cells were cultured in DMEM with 10% (v/v) fetal calf serum (FCS), 1% penicillin/streptomycin, and 1% L-glutamine. Early passage MycCaP or HeLa cells were plated in 12 well dishes (2.0×10^5 cells/well), and all experiments were performed 16 h later. Assays were initiated by the addition of an aliquot (50 μL) of ^{89}Zr-mTf (~900 kBq/mL [24 μCi/mL]) to cells maintained in 450 μL of DMEM containing 10% FCS. At the indicated times, media was removed, cells were washed twice (2×500 μL) with PBS, and the aliquots were combined. Cells were then incubated (500 μL) with an acidic solution (100 mM glycine, 10 mM acetic acid, pH 3.0) for 1 min. to strip surface bound radiotracer. The acidic wash was stored as a separate aliquot. Finally, cells were lysed in 500 μL of 0.1 M NaOH(aq.) to collect internalized activity. Radioactivity from the media, acidic, and alkali fractions was quantified by γ-counting, and after background correction, cell-associated activity was reported as a percentage of total activity per well, relative to control wells and normalised per 1×10^6 cells. To verify saturation and temperature dependence of radiotracer uptake, the assay was performed at multiple time points and at either 4 ºC or 37 ºC (n = 4/condition).

Genetic knockdown of AR by siRNA

MycCaP and MycCaP + CMVmyc cells were plated in 6 well dishes (4.0×10^5 cells/well) and 16 h later, cells were transfected with pools of non-targeting (NT) or AR-directed siRNAs (Dharmacon) with the DharmaFECT™ reagent (Dharmacon)[8]. Cells were harvested 24 h post-transfection, RNA isolated (QIAGEN), and cDNA prepared (Applied Biosystems, Inc.). Expression levels of murine AR, *c-Myc*, and TFRC were determined by qPCR using commercially available primers (Superarray Biosciences).

Histology

Staining and microscopy was performed by the Memorial Sloan-Kettering Cancer Center (MSKCC) Histology Core facility using standard methods.

Xenograft models

All animal experiments were conducted in compliance with Institutional Animal Care and Use Committee (IACUC) guidelines and the *Guide for the Care and Use of Laboratory Animals*[9]. Immunocompetent male FVB mice (6–8 weeks old) were obtained from Taconic Farms Inc. (Hudson, NY), and were allowed to acclimatize at the MSKCC vivarium for 1 week prior to implanting tumors. Mice were provided with food and water *ad libitum*. MycCap tumors were induced on the right flank by sub-cutaneous (s.c.) injection of 2.0×10^5 cells in a 200 μL cell suspension of a 1:1 v/v mixture of media with reconstituted basement membrane (BD Matrigel™, Collaborative Biomedical Products Inc., Bedford, MA). Palpable MycCap tumors (50–250 mm^3) developed after a period of 14–21 days. Surgical castration was performed according to our protocol under anesthesia with isoflurane. Tumor volume (V / mm^3) was estimated by external vernier caliper measurements in accordance with previously reported methods[5]. Analysis of gene transcript levels of MycCaP xenografts from intact and castrate hosts was performed by isolating RNA from xenograft tissue with Trizol extraction (Invitrogen), cDNA production, and qPCR (*vide supra*).

Genetically engineered mouse (GEM) models

GEM models of human prostate cancer (Hi-Myc mice at 4 and 12 months old) used in these experiments were maintained in the MSKCC animal housing facility in accordance with approved IACUC protocols. Genotyping was conducted by the MSKCC Core facility using previously published primer sets and protocols[10]. Hi-Myc mice were aged to either 4 or 12 months prior to use in this study. At the completion of experiments mice were euthanized by CO_2 asphyxiation and tissue was procured for histology, mRNA analysis, and protein analysis.

Inflammation model

Mouse models of inflammation were developed by s.c. injection of turpentine oil (50 μL, neat) on one of the hind limbs of intact, immunocompetent male FVB mice. Inflammation developed rapidly and mice were subjected to PET imaging 24 – 48 h post-administration of turpentine.

Biodistribution studies

Biodistribution studies were conducted to evaluate the uptake of ^{89}Zr-mTf in immunocompetent FVB mice bearing s.c. MycCaP tumors (average volume = 85±15 mm^3). Mice were randomized before the study and 48 h prior to administering ^{89}Zr-mTf, one cohort was castrated. Mice were warmed gently with a heat lamp 5 min. before administering ^{89}Zr-mTf (0.55–0.74 MBq, [15–20 μCi], 1.7–2.2 μg of mTf, in 200 μL sterile saline for injection) *via* intravenous (i.v.) tail-vein injection (t=0 h). Animals (n=4–5, per group) were euthanized by CO_2(g) asphyxiation at 1, 5, and 24 h post-injection and 16 tissues (including the tumor) were removed, rinsed in water, dried in air for 5 min., weighed and counted on a calibrated gamma-counter for accumulation of ^{89}Zr-radioactivity. The mass of ^{89}Zr-mTf formulation injected into each animal was measured and used to determine the total number of counts (counts per minute, [c.p.m.]) by comparison to a standard syringe of known activity and mass. Count data were background- and decay-corrected and the tissue uptake measured in units of percentage injected dose per gram (%ID/g) for each sample was calculated by normalization to the total amount of activity injected.

Small-animal PET imaging

PET imaging experiments were conducted on a microPET Focus 120 scanner (Concorde Microsystems). In repeated studies (n = 4), mice were administered formulations of ^{89}Zr-mTf (11.6–13.7 MBq, [313–370 μCi], 35–41 μg of protein, in 200 μL sterile saline for injection) *via* i.v. tail-vein injection. Equivalent amounts of activity were administered for PET imaging with ^{89}Zr-hTf and ^{89}Zr-mAlb. Approximately 5 minutes prior to recording PET images, mice were anesthetized by inhalation of 1–2% isoflurane (Baxter Healthcare, Deerfield, IL)/oxygen gas mixture and placed on the scanner bed. PET images were recorded at various time-points between 1 – 120 h post-injection. List-mode data were acquired for between 10 and 30 min. using a γ-ray energy window of 350–750 keV, and a coincidence timing window of 6 ns. For all static images, scan time was adjusted to ensure a minimum of 20 million coincident events were recorded. Data were sorted into 2-dimensional histograms by Fourier re-binning, and transverse images were reconstructed by filtered back-projection (FBP) into a 128×128×63 (0.72×0.72×1.3 mm) matrix. The reconstructed spatial resolution for ^{89}Zr was 1.9 mm full-width half maximum (FWHM) at the center of the field-of-view (FOV). Image data were normalised to correct for non-uniformity of response of the PET, dead-time count losses, positron branching ratio, and

physical decay to the time of injection, but no attenuation, scatter, or partial-volume averaging correction was applied. An empirically determined system calibration factor (in units of [mCi/mL]/[cps/voxel]) for mice was used to convert voxel count rates to activity concentrations. The resulting image data were then normalised to the administered activity to parameterise images in terms of %ID/g. Manually drawn 2-dimensional regions-of-interest (ROIs) or 3-dimensional volumes-of-interest (VOIs) were used to determined the maximum and mean %ID/g (decay corrected to the time of injection) in various tissues. Images were analyzed by using ASIPro VM^{TM} software (Concorde Microsystems).

For all *in vivo* studies involving Hi-Myc transgenic animals and WT controls, end time point biodistribution studies were also performed harvesting 21 tissues. Specific uptake of ^{89}Zr-mTf in local prostatic adenocarcinoma was also demonstrated in Hi-Myc (12 mo) animals (n = 4) by the use of blocking studies. For blocking experiments, mice were administered a high dose of non-radiolabelled holo-Tf (200 mg/kg; 100 μL in sterile saline) *via* i.v. tail vein injection at 45 min. prior to ^{89}Zr-mTf administration. Details of the radiotracer preparation and dose formulation for the blocked mice were identical to those used for imaging non-blocked Hi-Myc and WT mice (*vide supra*). Temporal PET imaging *in vivo*, as wells as *ex vivo* PET imaging of the prostate micro-dissection and full biodistribution studies were conducted at 24 h post-radiotracer administration.

Co-registered PET/CT

Computed tomography (CT) images were acquired on a small-animal Siemens/CTI microCAT II (Siemens Medical Solutions, Malvern, PA) scanner with an 8.5 cm axial by 5.0 cm transaxial FOV. Co-registered PET/CT images were recorded at 16 h post-radiotracer administration. Images from the two separate modalities were mapped to a matrix and co-registered in accordance with previously reported methods[11].

Magnetic resonance (MR) imaging

Mouse prostate MR images were acquired on a Bruker 4.7T Biospec scanner operating at 200 MHz and equipped with a 400 mT/m ID 12 cm gradient coil (Bruker Biospin MRI, GmbH, Ettlingen, Germany). A custom-built quadrature birdcage resonator with ID of 32 mm was used

for RF excitation and acquisition (Stark Contrast MRI Coils Research Inc., Erlangen, Germany). Mice were anaesthetized with oxygen and 1–2% isoflurane gas/oxygen mixture. Animal breathing was monitored by using a small animal physiological monitoring system (SA Instruments, Inc., Stony Brook, New York). T_2 weighted scout images along three orthogonal orientations were first acquired for animal positioning. The T_2-weighted fast spin-echo RARE sequence (Rapid Acquisition with Relaxation Enhancement) was used to acquire axial mouse pelvic images with a slice thickness of 0.8 mm, FOV 30 mm × 34 mm with a spatial resolution of 117 μm × 133 μm. The following acquisition parameters, TR = 4.5 s, TE= 40 ms, RARE factor 8, and an acquisition time of 20 minutes were used.

Biological half-life

The biological half-life of ^{89}Zr-mTf was measured in Hi-Myc (12 mo) transgenic animals and SCID mice (Taconic Farms Inc.). Mice (n = 4/strain) were administered ^{89}Zr-mTf (Hi-Myc mice: 11.8–12.8 MBq, [319–346 μCi], 36–39 μg of protein; SCID mice: 8.3–10.0 MBq, [223–271 μCi], 25–30 μg of protein) and total internal radioactivity was measured as a function of time by using a dose calibrator.

Statistical analyses

Data were analysed by using the unpaired, two-tailed Student's t-test. Differences at the 95% confidence level (P<0.05) were considered to be statistically significant.

Results

Supplementary Figure 2. Radio-ITLC data for ^{89}Zr-Tf radiolabeling

Typical radio-ITLC chromatograms of the crude (red) and purified (blue) ^{89}Zr-mTf. Eluent: DTPA(aq.), 50 mM, pH7. NB: The normalised count data for the chromatogram of the crude product (red) is offset by 1 unit for clarity. ^{89}Zr-mTf remains at the baseline (R_f = 0.0) and impurities run with solvent (R_f = 1.0). Equivalent results were obtained for ^{89}Zr-hTf and ^{89}Zr-mAlb.

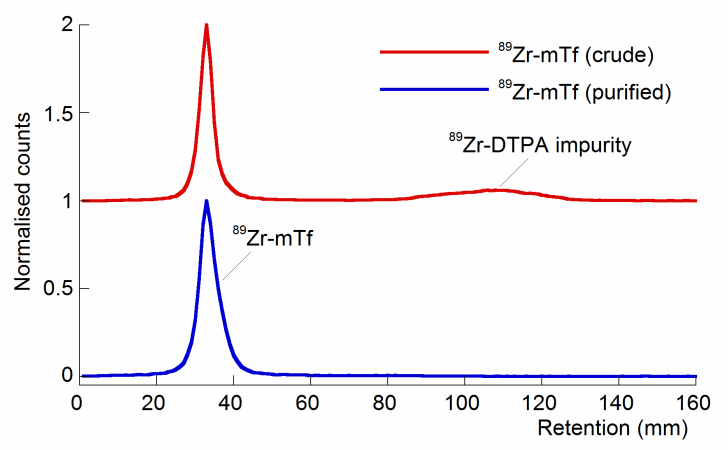

Supplementary Figure 3. Size-exclusion chromatography for radiotracer purification

Typical elution profiles observed using PD-10 size-exclusion chromatography for the analytical characterisation and purification of ^{89}Zr-mTf from small molecule (<30 kDa) ^{89}Zr-radiolabelled impurities and unreacted ^{89}Zr-oxalate (complexed as ^{89}Zr-DTPA). Species with MW >30 kDa elute in the first 1.8 mL of solvent. NB: the first 2.5 mL loading volume was discarded prior to collecting fractions. Equivalent results were obtained for ^{89}Zr-hTf and ^{89}Zr-mAlb.

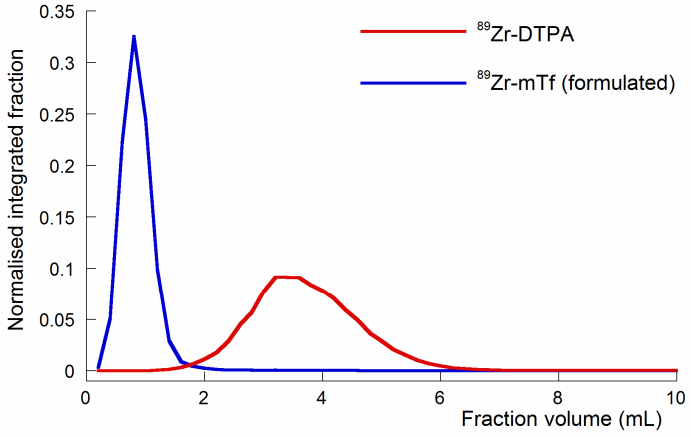

Supplementary Table 1. *In vitro* stability studies

The stability of ^{89}Zr-mTf, ^{89}Zr-mTf and ^{89}Zr-mAlb with respect to a decrease in radiochemical purity (RCP) associated with the loss of radionuclide from the protein/DFO-chelate and was assessed by using radio-ITLC and γ-counting[12]. All solutions were incubated at 37 ºC and ITLC strips were developed using 50 mM DTPA(aq.) as the mobile phase solvent.[a]

		Percentage baseline activity / % at time, *t* / h			
Radiotracer	**Solution**	**0 h**	**24 h**	**72 h**	**120 h**
^{89}Zr-mTf	Saline	100	100	99 ± 1	99 ± 1
	PBS	100	99 ± 1	99 ± 1	100
^{89}Zr-hTf	Saline	100	100	100	100
	PBS	100	100	98 ± 2	99 ± 1
^{89}Zr-mAlb	Saline	100	NM[b]	98 ± 1	99 ± 1
	PBS	100	NM[b]	99 ± 1	98 ± 1

[a] In this experiment using DTPA as the mobile phase, $^{89}Zr^{4+}$ ions in solution or non-specifically bound to the protein coordinate rapidly with the DTPA ligand and migrate with the solvent front (R_f = 1.0). Activity at the baseline (R_f = 0.0) is indicative of specifically radiolabelled ^{89}Zr-DFO-Tf. [b] NM = not measured.

Fe^{3+}-coordination challenge

For the preparation of the radiolabelled holo-Tf constructs, ^{89}Zr-mTf(holo) and ^{89}Zr-hTf(holo), the purified (RCP >99%) apo-radiotracers were incubated in a solution of excess $FeCl_3$(aq.) (>10 mM, 16 h at room temperature). After incubation, the Fe-loaded radiotracers ^{89}Zr-mTf(holo) and ^{89}Zr-hTf(holo) were purified from excess Fe^{3+}(aq.) by the use of size exclusion spin column centrifugation (*vide supra*). During the Fe-loading reaction, we noted no loss of $^{89}Zr^{4+}$ from the construct indicating that under these challenging reaction conditions with excess Fe^{3+}, no transmetallation (and associated loss of RCP) occurred. Hence, these data support the conclusion that the ^{89}Zr-DFO coordination complex is thermodynamically and kinetically more stable than the corresponding Fe-DFO complex.

Supplementary Figure 4. *In vitro* and *in vivo* HPLC metabolism studies

Size-exclusion radio-HPLC chromatograms (plotted as cumulative fraction of total activity *versus* elution volume / mL) for incubation of (**a**) ^{89}Zr-mTf in saline, (**b**) ^{89}Zr-hTf in saline, (**c**) ^{89}Zr-mTf in human blood, (**d**) ^{89}Zr-hTf in human blood, (**e**) ^{89}Zr-mTf in mouse urine *in vivo*, and (**f**) ^{89}Zr-mTf in mouse blood *in vivo*, at 24, 48 and 96 h post-administration of the radiotracers.

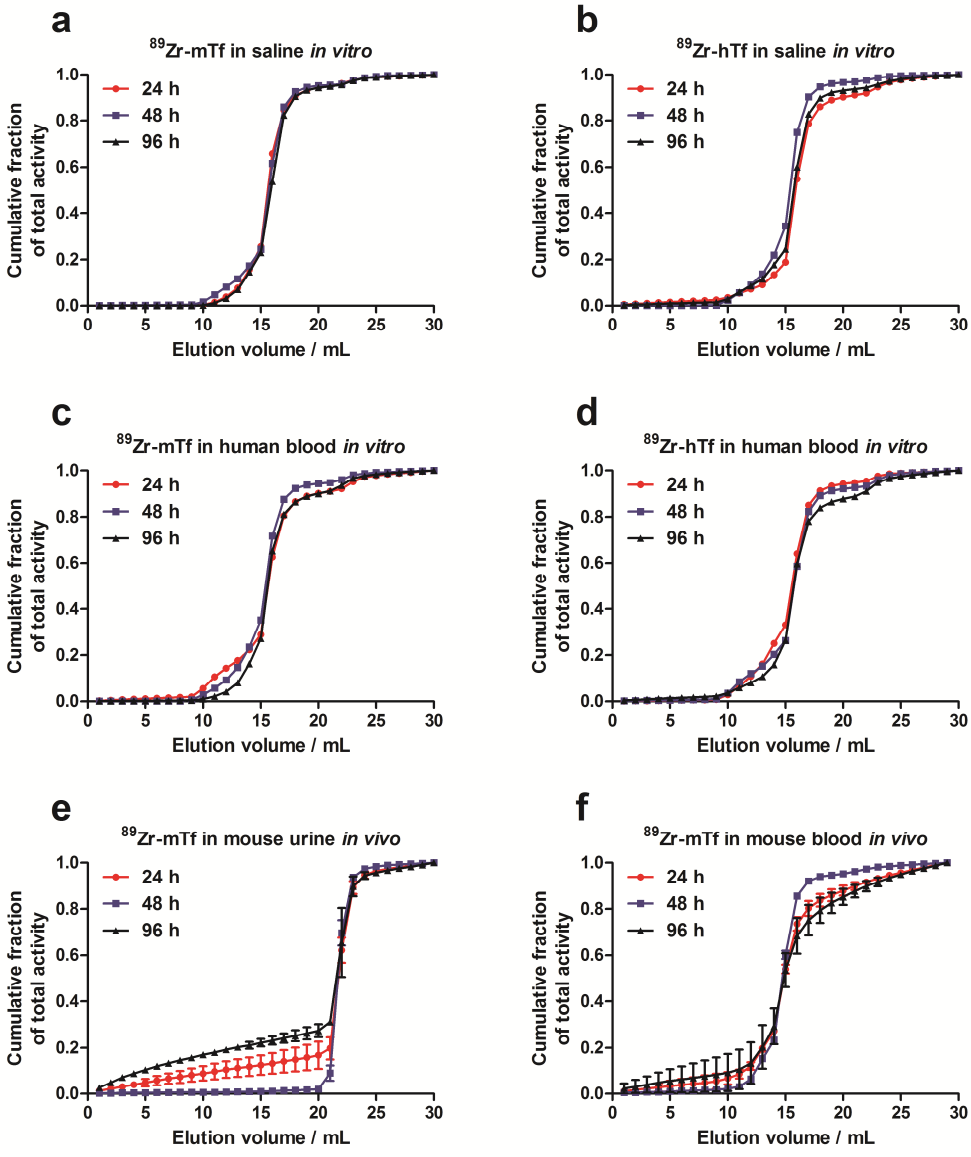

Brief, radio-HPLC metabolism and stability studies indicate that ^{89}Zr-mTf and ^{89}Zr-hTf are stable with respect to aggregation, metabolism or loss of the ^{89}Zr-activity for up to 96 h in saline and human blood *in vitro*. Metabolism analysis from *in vivo* samples also confirm that ^{89}Zr-mTf

remains stable with respect to aggregation, transmetallation or metabolism in the blood with >80% RCP at 96 h with no small-molecule metabolites observed in the blood pool. As expected, ^{89}Zr-radioactivity excreted in the urine is composed of small molecule metabolites of as yet unknown chemical composition. We note that in our previous studies on ^{89}Zr-radiolabelled mAbs and chelates, the $[^{89}Zr(DFO)(H_2O)_2]^{2+}$ complex displayed rapid blood pool clearance and renal excretion with a biological half-life $t_{1/2.biol}$ ~5 min. for bladder filling. As such the $[^{89}Zr(DFO)(H_2O)_2]^{2+}$complex represents one plausible metabolite (formed by amide bond hydrolysis of the linker) found in the urine[4].

Supplementary Figure 5. Measurement of the effective and biological half-life of ^{89}Zr-mTf
Plot of the normalised (mean) change in total internal radioactivity in Hi-Myc (12 mo) *versus* time / h from which the effective (measured) and biological half-life of ^{89}Zr-mTf can be extrapolated by non-linear regression analysis fitted with a exponential decay model (correlation coefficient, R^2 = 0.98). These data indicate that radioactivity administered as ^{89}Zr-mTf is effectively cleared from the body at a rate ~1.7 times faster than physical decay of the ^{89}Zr radionuclide. Metabolism studies, PET imaging and biodistribution experiments (*vide infra*) confirm that renal as opposed to hepatobiliary clearance is the primary route of excretion of the ^{89}Zr radioactivity.

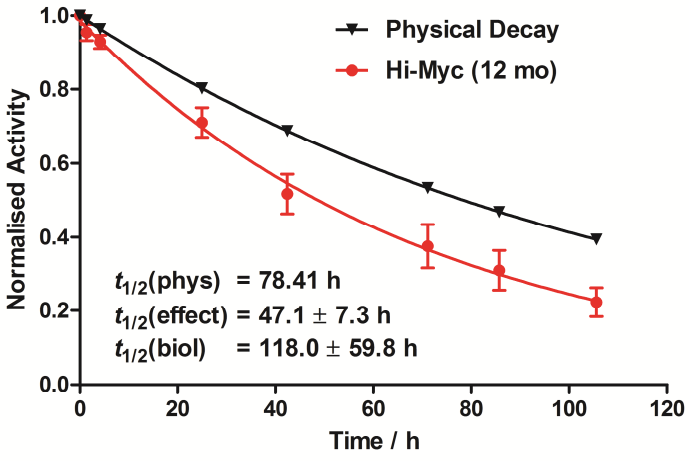

Supplementary Figure 6. Cellular uptake of ^{89}Zr-hTf and ^{89}Zr-mTf in MycCaP and HeLa cells

Cellular uptake of ^{89}Zr-mTf and ^{89}Zr-hTf in MycCaP and HeLa cells, respectively, using the apo-transferrin and Fe^{3+}-loaded holo-transferrin radiotracers. Fe^{3+} loading of the ^{89}Zr-Tf led to increased cellular uptake consistent with the well-known biochemical mechanism and increased binding affinity of holo-transferrin for TFRC. In each case, the majority of the ^{89}Zr-activity was found to be internalised, consistent with the well-established biochemical mechanism of Tf-TRFC binding and Fe uptake. NB: Uptake data in 1×10^6 cells are normalised to the total amount of activity in control wells. Normalisation for protein content gave equivalent results.

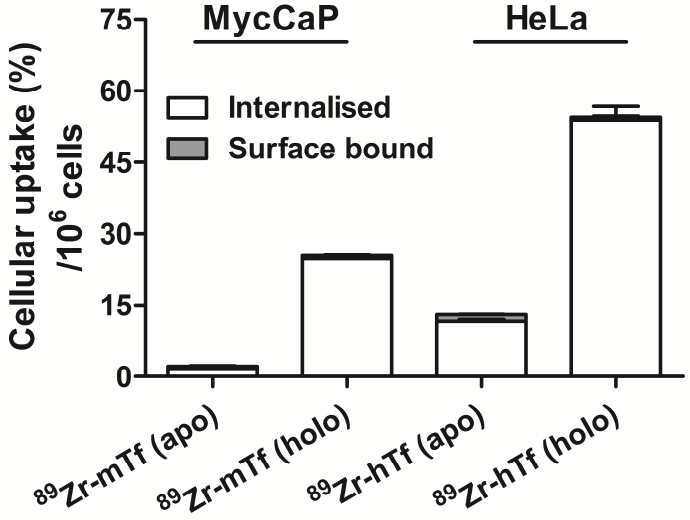

Supplementary Figure 7. PET imaging of inflammation

Representative temporal PET images from 1 – 24 h post-i.v. administration of (**a**) ^{89}Zr-mTf, (**b**) ^{89}Zr-hTf, and (**c**) ^{89}Zr-mAlb in mice with inflamed right hind limbs induced by s.c. injection of turpentine oil (50 µL; 20 h prior to radiotracer administration). ^{89}Zr-mAlb PET imaging demonstrates the low signal accumulation observed from non-targeted enhanced permeability and retention (EPR) effects for a protein construct of similar size, shape and overall charge.

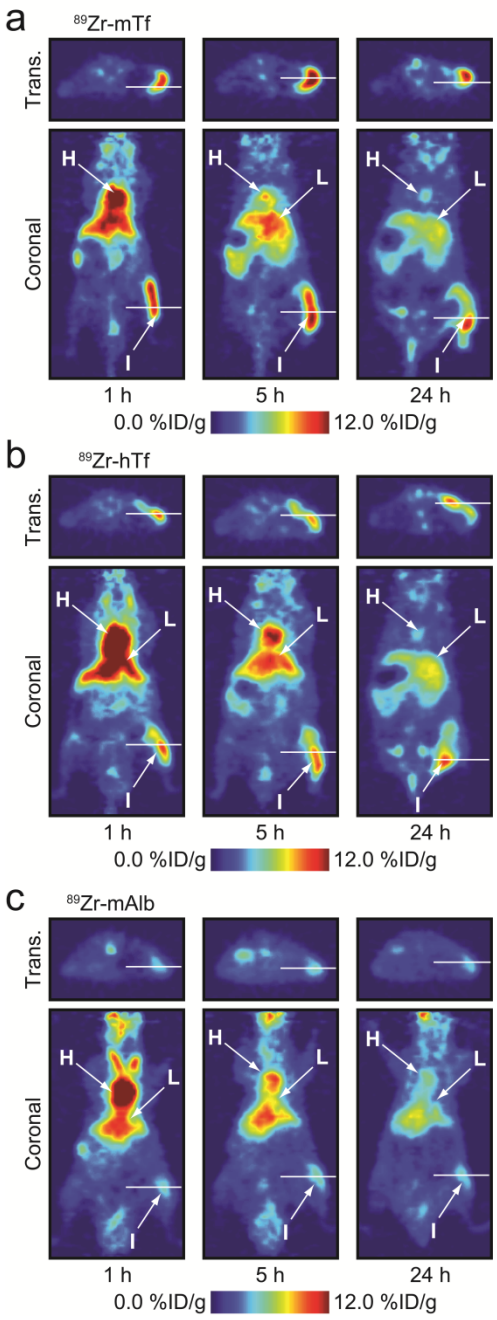

Supplementary Table 2. Biodistribution data for radiotracer uptake in the inflammation model

Ex vivo biodistribution data for ^{89}Zr-mTf (n = 5), ^{89}Zr-hTf (n = 5) and ^{89}Zr-mAlb (n = 2) radiotracers at 24 h post-i.v. administration in immunocompetent male FVB mice treated with turpentine oil in the right hind limb to induce inflammation (50 μL; sub-cutaneous injection 20 h prior to radiotracer administration).[a]

Organ	**^{89}Zr-mTf** (20 – 22 μg mTf) 24 h (n = 5)	**^{89}Zr-hTf** (36 – 37 μg hTf) 24 h (n = 5)	**^{89}Zr-mAlb** (29 – 32 μg mAlb) 24 h (n = 2)
Blood	4.3 ± 0.3	4.5 ± 0.4	7.1 ± 0.3
Heart	2.6 ± 0.3	2.5 ± 0.5	3.7 ± 0.4
Lungs	2.2 ± 0.3	1.8 ± 0.8	3.5 ± 0.1
Liver	7.1 ± 0.8	5.2 ± 1.2	7.7 ± 1.8
Spleen	3.2 ± 0.9	2.7 ± 0.8	2.9 ± 0.3
Stomach	0.6 ± 0.1	0.8 ± 0.1	1.1 ± 0.2
Small Intestine	1.1 ± 0.1	1.0 ± 0.1	1.4 ± 0.2
Large Intestine	2.1 ± 0.4	2.5 ± 0.7	1.8 ± 0.1
Kidneys	6.6 ± 0.8	4.0 ± 1.0	10.3 ± 0.2
Testes	2.1 ± 0.4	2.1 ± 0.5	1.9 ± 0.1
Bladder	2.6 ± 0.7	2.6 ± 0.5	3.3 ± 0.4
Inflamed Muscle [b]	3.3 ± 0.8	3.3 ± 0.8	0.4 ± 0.1
Control Muscle [c]	0.5 ± 0.1	0.5 ± 0.2	0.5 ± 0.03
Bone	6.6 ± 1.4	6.0 ± 1.7	1.5 ± 0.2
Inflamed muscle (IM) to tissue uptake ratios [d]			
IM/Blood	0.78 ± 0.20	0.75 ± 0.18	0.06 ± 0.02
IM/Heart	1.29 ± 0.35	1.34 ± 0.41	0.12 ± 0.03
IM/Lungs	1.51 ± 0.43	1.86 ± 0.96	0.12 ± 0.03
IM/Liver	0.47 ± 0.13	0.64 ± 0.21	0.06 ± 0.02
IM/Spleen	1.03 ± 0.39	1.25 ± 0.46	0.15 ± 0.04
IM/Stomach	5.39 ± 1.59	4.27 ± 1.27	0.39 ± 0.11
IM/Sm. Intestine	3.01 ± 0.79	3.35 ± 0.87	0.31 ± 0.09
IM/L. Intestine	1.59 ± 0.48	1.33 ± 0.49	0.24 ± 0.06
IM/Kidneys	0.50 ± 0.14	0.84 ± 0.28	0.04 ± 0.01
IM/Testes	1.58 ± 0.50	1.58 ± 0.51	0.24 ± 0.06
IM/Bladder	1.29 ± 0.48	1.26 ± 0.37	0.13 ± 0.04
IM/Control Muscle	6.63 ± 1.91	6.71 ± 2.92	0.88 ± 0.23
IM/Bone	0.51 ± 0.17	0.56 ± 0.20	0.30 ± 0.08

[a] Data are expressed as the mean %ID/g ± one standard deviation (S.D.) [b] Inflamed muscle taken from the right hind limb. [c] Control muscle taken from the contralateral left hind limb.[d] Errors for the inflamed muscle-to-tissue ratios are calculated as the geometric mean of the standard deviations.

Supplementary Figure 8. Biodistribution plot – Inflammation model

Bar chart showing selected tissue biodistribution data (%ID/g) for the uptake of ^{89}Zr-mTf (n = 5), ^{89}Zr-hTf (n = 5) and ^{89}Zr-mAlb (n = 2) radiotracers at 24 h post-i.v. administration in immunocompetent male FVB mice treated with turpentine oil in the right hind limb to induce inflammation (50 μL; sub-cutaneous injection 20 h prior to radiotracer administration). *, P-values for radiotracer uptake in inflamed (right) *versus* contralateral control muscle (left): ^{89}Zr-mTf = 0.0015; ^{89}Zr-hTf = 0.0008; and ^{89}Zr-mAlb = 0.59. Int = intestine.

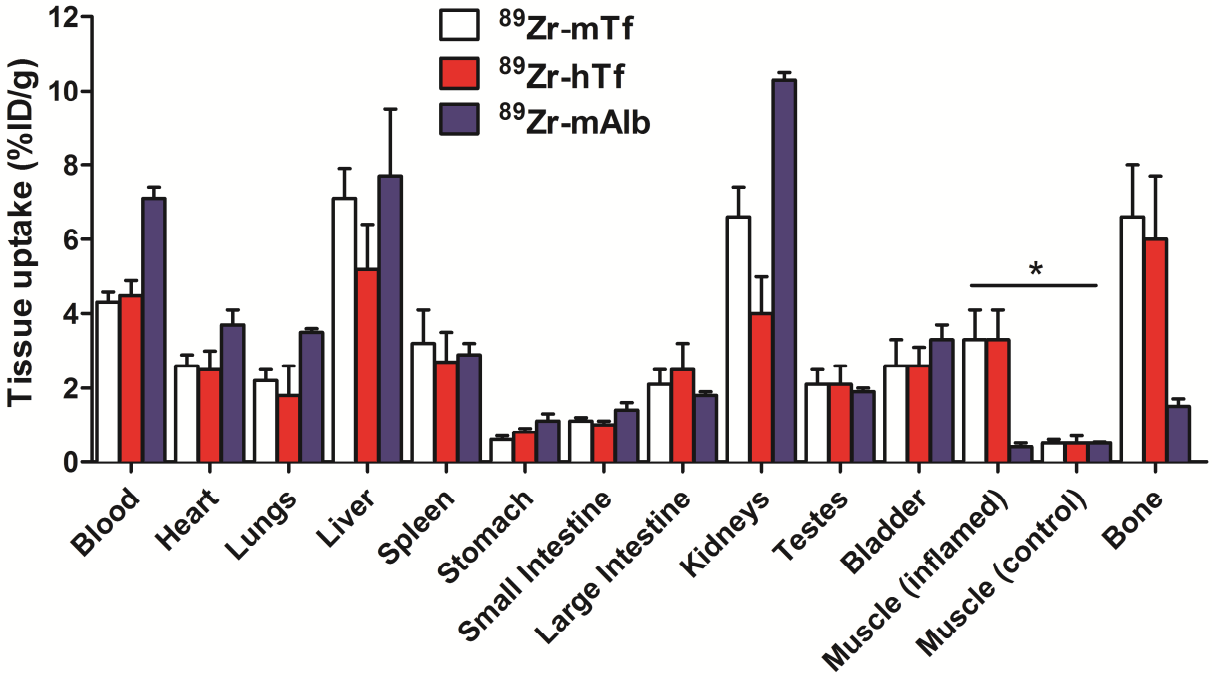

Supplementary Figure 9. Quantitative-PCR on MycCaP xenograft tissue from intact and castrated models

qPCR data demonstrating a statistically significant ($P < 0.001$) decrease in both *c*-Myc and TFRC levels in MycCaP xenograft tissue from intact and castrated (48 h prior to sacrifice) mice ($n = 4$/group).

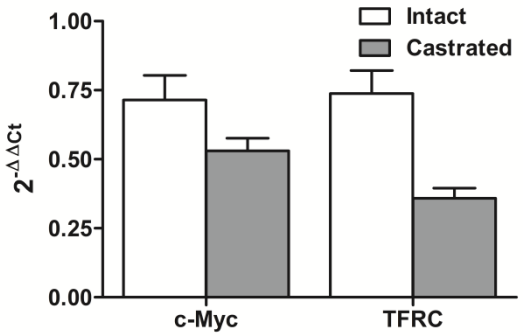

Supplementary Figure 10. Quantitative-PCR on MycCaP+Myc cells

qPCR data showing the relative gene expression levels of androgen receptor (AR), transgene *c*-Myc, and TFRC 48 h after treating MycCaP+Myc cells (constitutively expressing *c*-Myc) with either non-targeted (NT) or AR-directed siRNAs.

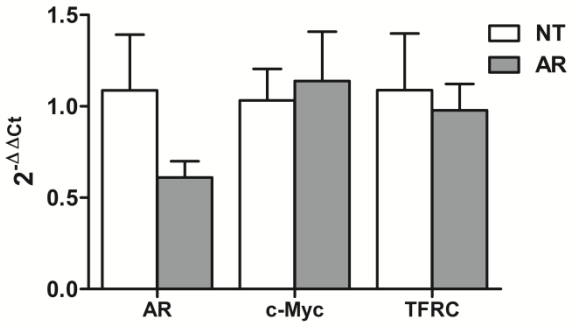

Supplementary Figure 11. ^{18}F-FDG PET imaging of MycCaP xenografts

^{18}F-FDG PET imaging of intact, WT FVB mice bearing s.c. MycCaP tumors on the right flank. ^{18}F-FDG PET data confirm that MycCaP tumors are viable and metabolically active but also highlight the inadequacies associated with ^{18}F-FDG for imaging the prostate. High renal excretion and accumulation of ^{18}F-radioactivity in the bladder precludes imaging and analysis of radiotracer distribution in the abdominal region. H = heart; L = liver; B = bladder.

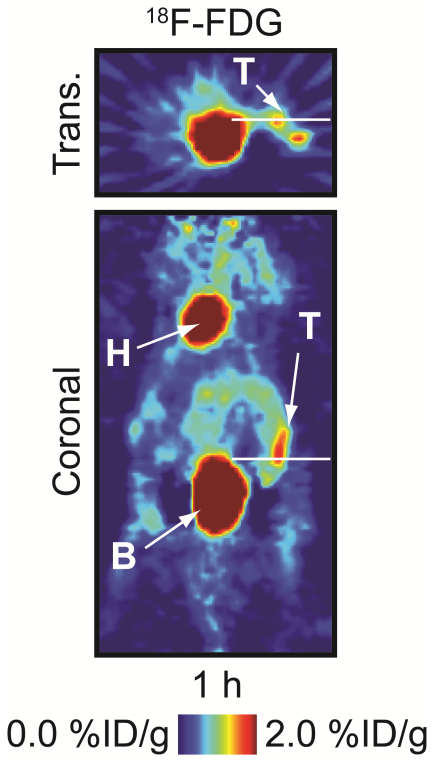

Supplementary Table 3. Biodistribution data for ^{89}Zr-mTf uptake in *intact* MycCaP tumor-bearing mice

Ex vivo biodistribution data for ^{89}Zr-mTf (0.55–0.74 MBq, [15–20 μCi], 1.7–2.2 μg of protein/mouse) uptake in intact immunocompetent male FVB mice bearing s.c. MycCaP xenografts at 1, 5 and 24 h post-i.v. administration.[a]

Organ	1 h (*n* = 4)	5 h (*n* = 4)	24 h (*n* = 4)
Intact FVB mice			
Blood	14.43 ± 1.25	14.67 ± 0.80	4.68 ± 0.32
Tumor	0.88 ± 0.27	3.14 ± 0.68	3.24 ± 0.28
Heart	3.60 ± 0.85	4.95 ± 0.97	2.02 ± 0.29
Lungs	9.15 ± 0.98	10.71 ± 1.86	3.83 ± 0.36
Liver	4.53 ± 0.88	5.53 ± 0.52	3.89 ± 0.57
Spleen	2.07 ± 0.12	2.65 ± 0.31	2.11 ± 0.41
Pancreas	0.88 ± 0.16	1.27 ± 0.22	0.88 ± 0.03
Stomach	1.01 ± 0.64	0.92 ± 0.18	0.64 ± 0.16
Small Int	1.50 ± 0.39	1.50 ± 0.23	0.80 ± 0.09
Large Int	0.88 ± 0.43	1.68 ± 0.41	1.07 ± 0.13
Kidneys	4.93 ± 0.31	7.82 ± 0.67	6.15 ± 0.66
Testes	1.48 ± 0.24	2.33 ± 0.30	1.75 ± 0.12
Skin	0.59 ± 0.12	1.48 ± 0.16	1.78 ± 0.15
Fat	0.24 ± 0.13	0.73 ± 0.32	0.37 ± 0.16
Muscle	0.32 ± 0.09	0.81 ± 0.12	0.46 ± 0.14
Bone	0.86 ± 0.37	1.94 ± 0.43	4.07 ± 1.13
Intact FVB mice tumor-to-tissue uptake ratios [b]			
Blood	0.1 ± 0.0	0.2 ± 0.0	0.7 ± 0.1
Tumor	1.0 ± 0.4	1.0 ± 0.3	1.0 ± 0.1
Heart	0.2 ± 0.1	0.6 ± 0.2	1.6 ± 0.3
Lungs	0.1 ± 0.0	0.3 ± 0.1	0.8 ± 0.1
Liver	0.2 ± 0.1	0.6 ± 0.1	0.8 ± 0.1
Spleen	0.4 ± 0.1	1.2 ± 0.3	1.5 ± 0.3
Pancreas	1.0 ± 0.4	2.5 ± 0.7	3.7 ± 0.3
Stomach	0.9 ± 0.6	3.4 ± 1.0	5.0 ± 1.3
Small Int	0.6 ± 0.2	2.1 ± 0.5	4.0 ± 0.6
Large Int	1.0 ± 0.6	1.9 ± 0.6	3.0 ± 0.5
Kidneys	0.2 ± 0.1	0.4 ± 0.1	0.5 ± 0.1
Testes	0.6 ± 0.2	1.3 ± 0.3	1.9 ± 0.2
Skin	1.5 ± 0.5	2.1 ± 0.5	1.8 ± 0.2
Fat	3.6 ± 2.2	4.3 ± 2.1	8.8 ± 3.9
Muscle	2.8 ± 1.1	3.9 ± 1.0	7.1 ± 2.3
Bone	1.0 ± 0.5	1.6 ± 0.5	0.8 ± 0.3

[a] Data are expressed as the mean %ID/g ± one standard deviation (S.D.) [b] Errors tumor-to-tissue uptake ratios are calculated as the geometric mean of the standard deviations. Int = intestine.

Supplementary Table 4. Biodistribution data for ^{89}Zr-mTf uptake in *castrated* MycCaP tumor-bearing mice

Ex vivo biodistribution data for ^{89}Zr-mTf (0.55–0.74 MBq, [15–20 μCi], 1.7–2.2 μg of protein/mouse) uptake in castrated immunocompetent male FVB mice bearing s.c. MycCaP xenografts at 1, 5 and 24 h post-i.v. administration.[a]

Organ	1 h (*n* = 5)	5 h (*n* = 5)	24 h (*n* = 5)
Castrated FVB mice			
Blood	17.54 ± 1.48	18.07 ± 1.11	5.53 ± 0.44
Tumor	0.91 ± 0.21	1.15 ± 0.36	1.32 ± 0.37
Heart	5.57 ± 1.60	5.66 ± 0.81	2.11 ± 0.25
Lungs	12.25 ± 0.67	11.07 ± 0.92	3.96 ± 0.54
Liver	5.27 ± 0.48	7.36 ± 0.51	4.90 ± 0.59
Spleen	1.94 ± 0.34	3.27 ± 0.12	2.34 ± 0.25
Pancreas	0.97 ± 0.22	1.85 ± 0.16	1.42 ± 0.28
Stomach	0.75 ± 0.60	1.19 ± 0.26	0.45 ± 0.16
Small Int	1.65 ± 0.25	2.03 ± 0.30	0.88 ± 0.24
Large Int	0.63 ± 0.23	1.91 ± 0.26	1.14 ± 0.13
Kidney (Both)	6.10 ± 0.67	8.78 ± 1.60	7.44 ± 0.76
Testes	N/A	N/A	N/A
Skin	0.52 ± 0.07	1.83 ± 0.25	2.28 ± 0.22
Fat	0.29 ± 0.14	1.27 ± 0.33	1.48 ± 0.33
Muscle	0.40 ± 0.14	0.89 ± 0.08	0.54 ± 0.15
Bone	0.95 ± 0.34	2.50 ± 0.25	3.55 ± 0.23
Castrated FVB mice tumor-to-tissue uptake ratios [b,c]			
Blood	0.1 ± 0.0	0.1 ± 0.0	0.2 ± 0.1
Tumor	1.0 ± 0.3	1.0 ± 0.4	1.0 ± 0.4
Heart	0.2 ± 0.1	0.2 ± 0.1	0.6 ± 0.2
Lungs	0.1 ± 0.0	0.1 ± 0.0	0.3 ± 0.1
Liver	0.2 ±0.0	0.2 ± 0.1	0.3 ± 0.1
Spleen	0.5 ±0.1	0.4 ± 0.1	0.6 ± 0.2
Pancreas	0.9 ± 0.3	0.6 ± 0.2	0.9 ± 0.3
Stomach	1.2 ± 1.0	1.0 ± 0.4	2.9 ± 1.3
Small Int	0.6 ± 0.2	0.6 ± 0.2	1.5 ± 0.6
Large Int	1.4 ± 0.6	0.6 ± 0.2	1.2 ± 0.4
Kidney (Both)	0.1 ± 0.0	0.1 ± 0.0	0.2 ± 0.1
Testes [c]	N/A	N/A	N/A
Skin	1.7 ± 0.5	0.6 ± 0.2	0.6 ± 0.2
Fat	3.2 ± 1.7	0.9 ± 0.4	0.9 ± 0.3
Muscle	2.3 ± 0.9	1.3 ± 0.4	2.4 ± 1.0
Bone	1.0 ± 0.4	0.5 ± 0.2	0.4 ± 0.1

[a] Data are expressed as the mean %ID/g ± one standard deviation (S.D.) [b] Errors on tumor-to-tissue uptake ratios are calculated as the geometric mean of the standard deviations. [c] Mice were castrated 48 h prior to radiotracer administration. Int = intestine.

Supplementary Figure 12. Biodistribution of ^{89}Zr-mTf in s.c. MycCaP tumor-bearing mice

Bar chart showing biodistribution data (%ID/g) for the uptake of ^{89}Zr-mTf at 1, 5 and 24 h post-i.v. administration in both castrated and intact immunocompetent FVB mice. *, *P*-values for tumor uptake in castrated *versus* intact mice: 1 h = 0.87; 5 h = 0.005; 24 h = 0.00005.

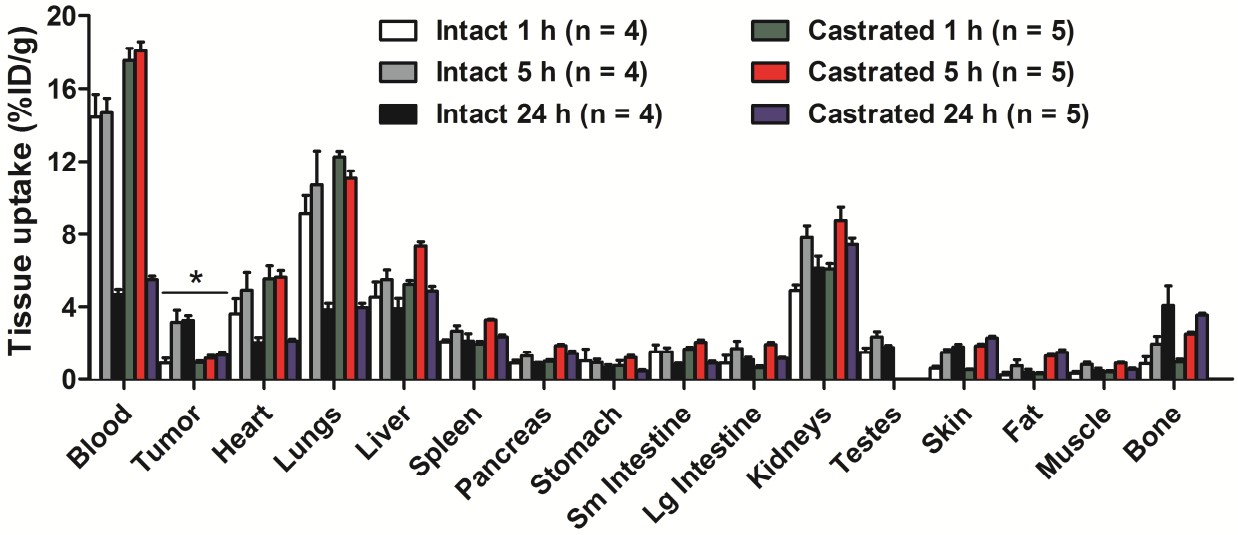

Supplementary Figure 13. Representative MRI slices of Hi-Myc (12 month) and WT mice prior to PET imaging with ^{89}Zr-mTf

Comparison between MRI images of Hi-Myc (12 mo) and age matched WT immunocompetent FVB mice showing advanced adenocarcinoma and enlarged prostate in the Hi-Myc model. B = bladder; PCa = prostate cancer; NP = normal prostate; R = right; L = left.

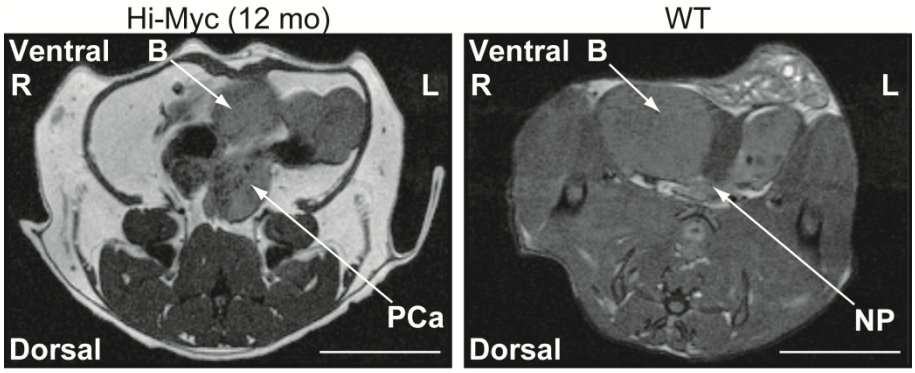

Volume analysis of the prostate tissue of Hi-Myc and WT animals from anatomical MRI gave mean sizes of 290±35 mm^3 for Hi-Myc (12 mo) mice (n = 6), and 110±25 mm^3 for WT FVB mice (n = 4). Hi-Myc (4 mo) mice have previously been shown to display no gross anatomical change in comparison with WT mice[10]. Tumor volumes measured by MRI are consistent with the average weights of prostates measured in the biodistribution studies: Hi-Myc mice = 0.285±0.045 g (n = 8); WT = 0.10±0.15 g.

Supplementary Figure 14. Representative dorsal-to-ventral stack plots of PET/CT imaging in Hi-Myc (12 month) mice

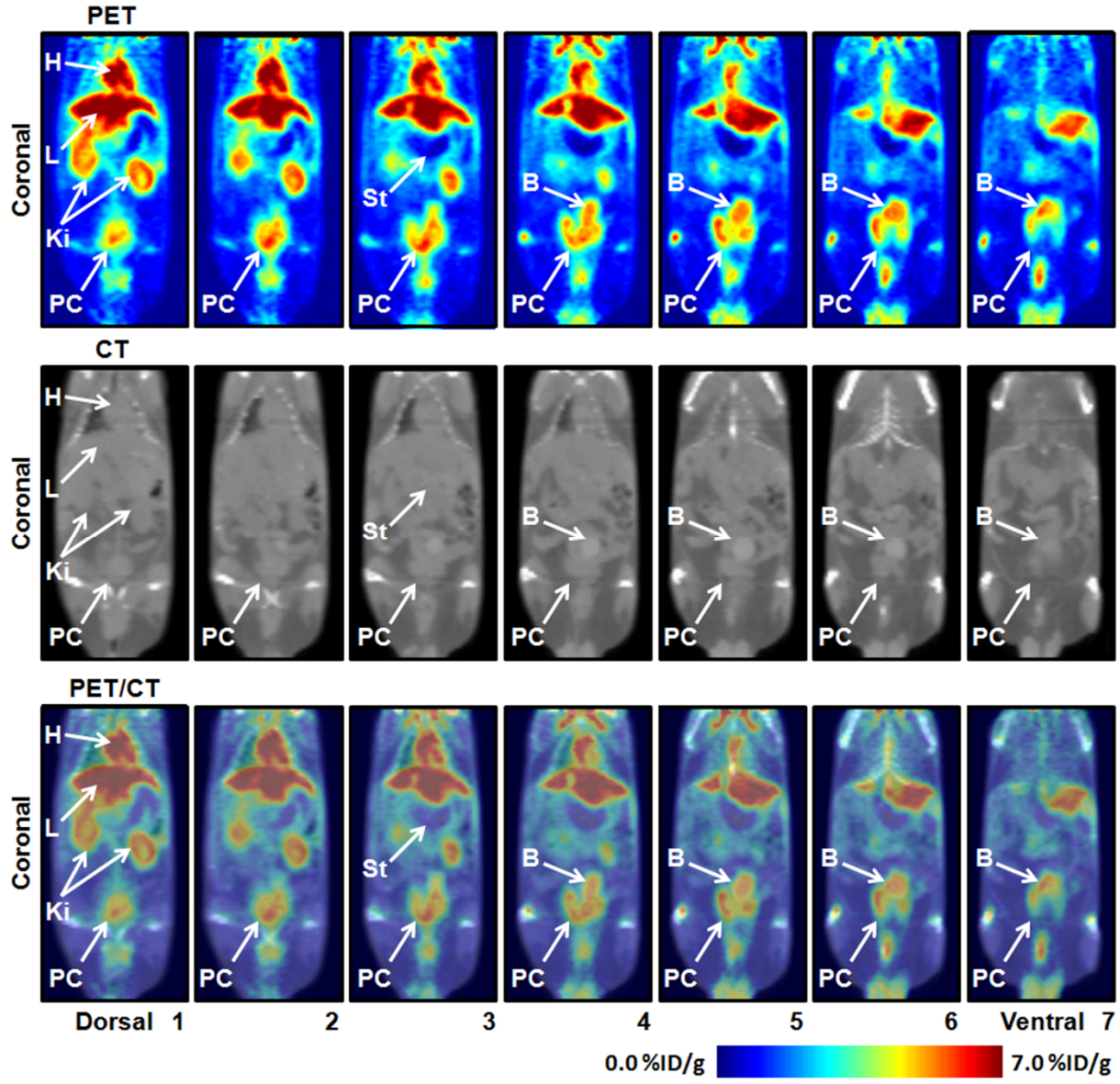

Supplementary Video 1. Maximum intensity projection (MIP) video of the ^{89}Zr-mTf PET image of the Hi-Myc (12 month) mouse shown in Figure 3.

The video shows the 3-dimensional distribution of ^{89}Zr-mTf at 16 h post-administration. The prostate and bladder are visible as spatially resolved masses showing high contrast in the lower abdomen. The figure below shows a maximum intensity projection (MIP) still image from the video.

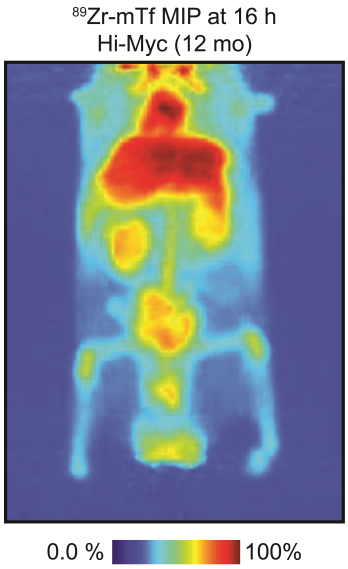

Supplementary Figure 15. Temporal PET imaging of ^{89}Zr-mTf in Hi-Myc (12 month) mice

Representative temporal PET images of ^{89}Zr-mTf distribution recorded in a Hi-Myc (12 mo) mouse between 4 – 120 h post-radiotracer administration. H = Heart; L = liver; PCa = prostate adenocarcinoma. The images show that ^{89}Zr-mTf is cleared from the background by ~120 h.

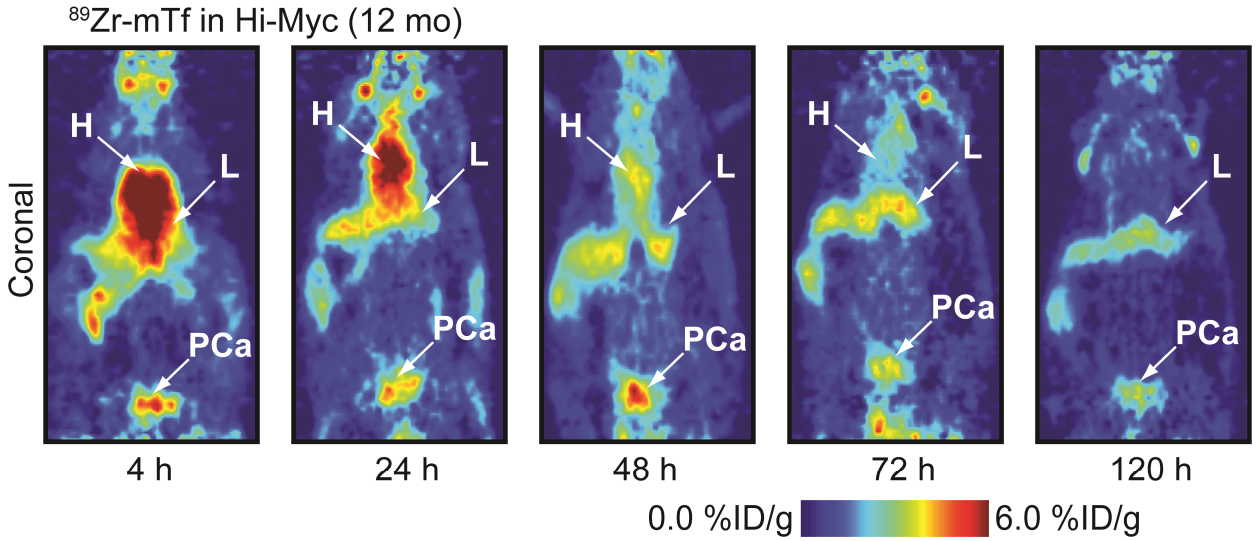

Supplementary Table 5. Quantitative VOI analysis of PET imaging data

Volume-of-interest analysis of PET images recorded at 24 h post-radiotracer administration prior to conducting biodistribution experiments (*vide supra*).

	Hi-Myc (12 mo) (*n* = 7)			**WT (*n* = 3)**			**Hi-Myc (12 mo) Block (*n* = 4)**		
Tissue	**Uptake %ID/g**	**SD**	***n*** [a]	**Uptake %ID/g**	**SD**	***n***	**Uptake %ID/g**	**SD**	***n***
Mean uptake data									
Prostate	4.75	0.38	6	1.99	0.44	5	2.40	0.13	8
Bladder	4.32	0.15	5	4.51	0.30	6	2.57	0.27	7
Heart	5.68	0.40	6	4.31	0.27	6	1.96	0.18	7
Liver	6.15	0.38	7	7.15	0.26	6	9.40	0.36	7
Muscle	0.65	0.08	5	0.40	0.06	7	0.35	0.01	5
Maximum uptake data									
Prostate	6.64	0.66	6	3.24	0.78	5	4.02	0.26	8
Bladder	6.06	0.80	5	7.42	0.19	6	3.71	0.09	7
Heart	7.68	0.45	6	5.95	0.36	6	2.80	0.21	7
Liver	7.96	0.40	7	10.33	0.79	6	16.40	1.24	7
Muscle	1.19	0.15	5	1.03	0.17	7	0.96	0.19	5

[a] *n* = number of 2-deimensional regions-of-interest (ROI) used in the VOI analysis.

Supplementary Figure 16. Quantitative analysis of PET imaging

Bart charts showing 3-dimensional volume-of-interest (VOI) analysis of ^{89}Zr-mTf uptake in various tissues based on PET images recorded 24 h post-radiotracer administration in Hi-Myc (12 mo) and WT mice. (**a**) Mean tissue uptake (%ID/g), and (**b**) maximum tissue uptake (%ID/g). * $P < 0.001$ for Student's *t*-test comparison between Hi-Myc (12 mo) animals and both WT and blocked groups.

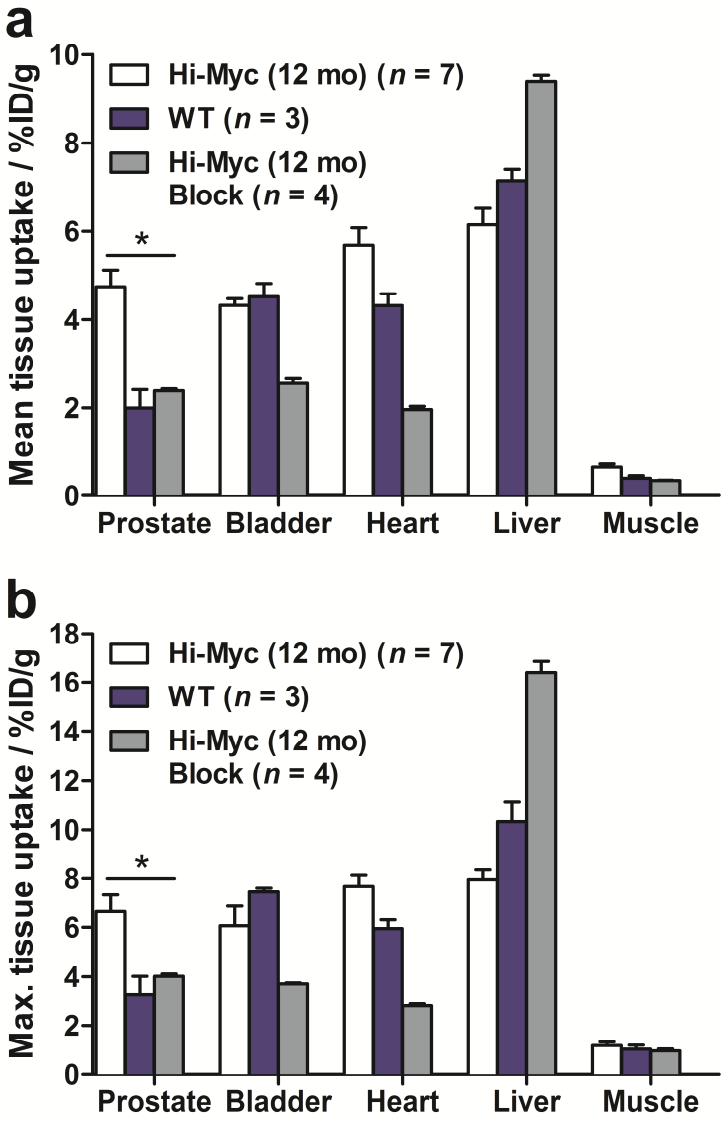

Supplementary Figure 17. Photograph of a urogenital tract micro-dissection for *ex vivo* PET

Representative photograph showing the excised urological tract from a Hi-Myc (12 mo) mouse. B = bladder; SV = seminal vesicles; AP = anterior prostate; DP = dorsal prostate; LP = lateral prostate; VP = ventral prostate. The ruler shows units in centimeters.

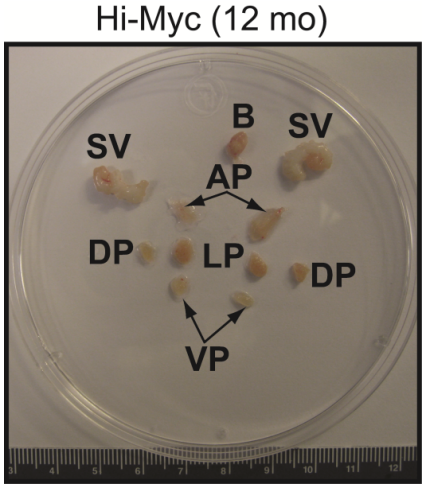

Supplementary Table 6. Biodistribution data for ^{89}Zr-mTf in Hi-Myc and WT mice

Ex vivo biodistribution data showing the uptake of ^{89}Zr-mTf (11.6–13.7 MBq, [313–370 μCi], 35–41 μg of protein/mouse) in Hi-Myc (12 mo and 4 mo), wild-type (WT) immunocompetent male FVB mice, as well as a blocking study in Hi-Myc (12 mo; 200 mg/kg non-radiolabelled holo-Tf) at 24 h post-i.v. administration of the radiotracer.[a]

Organ	Hi-Myc (12 mo) mice 24 h (*n* = 4)	Hi-Myc (4 mo) mice 24 h (*n* = 4)	WT mice 24 h (*n* = 3)	Hi-Myc (12 mo) mice Block 24 h (*n* = 4) [d]
Blood	4.5 ± 0.4	3.2 ± 0.2	5.2 ± 0.4	4.4 ± 0.9
Heart	2.6 ± 0.5	1.7 ± 0.1	3.4 ± 0.3	1.9 ± 0.3
Lungs	4.2 ± 0.9	3.5 ± 0.8	4.9 ± 0.3	2.2 ± 0.5
Liver	8.6 ± 1.1	11.4 ± 0.8	10.1 ± 0.8	12.9 ± 2.7
Spleen	4.3 ± 0.5	6.3 ± 1.4	4.5 ± 1.0	5.7 ± 0.9
Stomach	1.0 ± 0.3	0.4 ± 0.2	1.1 ± 0.4	1.1 ± 0.1
Small Int	1.0 ± 0.2	0.5 ± 0.2	1.2 ± 0.03	0.8 ± 0.1
Large Int	1.7 ± 0.4	1.2 ± 0.2	2.3 ± 0.4	1.7 ± 0.3
Kidneys	5.9 ± 0.9	3.5 ± 0.6	6.4 ± 1.0	3.9 ± 0.5
Testes	2.8 ± 0.6	1.7 ± 0.2	3.1 ± 0.6	2.3 ± 0.3
Bladder	2.3 ± 0.4	1.7 ± 1.0	2.0 ± 0.4	2.2 ± 1.1
Anterior prostate	0.5 ± 0.03	0.2 ± 0.1	0.5 ± 0.1	0.7 ± 0.1
D/V/L prostate [b]	3.1 ± 0.2	0.9 ± 0.1	0.5 ± 0.2	1.6 ± 0.2
Skin	1.7 ± 0.4	1.0 ± 0.1	1.9 ± 0.2	0.5 ± 0.1
Pancreas	0.9 ± 0.2	0.5 ± 0.2	0.8 ± 0.04	–
Brain	0.1 ± 0.01	–	0.2 ± 0.01	0.1 ± 0.1
Tail	2.2 ± 0.8	–	2.0 ± 0.1	0.7 ± 0.1
Muscle	0.4 ± 0.1	0.4 ± 0.1	0.4 ± 0.03	0.4 ± 0.1
Bone	3.2 ± 1.4	3.0 ± 0.3	2.9 ± 0.9	1.2 ± 0.3
Seminal Vesicle	0.4 ± 0.1	0.1 ± 0.04	0.2 ± 0.03	0.7 ± 0.4
Fat	0.3 ± 0.1	0.3 ± 0.1	0.4 ± 0.04	0.50 ± 0.1
Tissue-to-muscle uptake ratios [c]				
Blood/Muscle	10.4 ± 3.1	8.9 ± 3.3	12.5 ± 1.4	3.6 ± 1.1
Heart/Muscle	6.1 ± 2.1	4.6 ± 1.7	8.2 ± 1.0	1.6 ± 0.4
Lungs/Muscle	9.7 ± 3.4	9.6 ± 4.2	11.9 ± 1.1	1.8 ± 0.6
Liver/Muscle	19.8 ± 6.0	31.5 ± 11.8	24.5 ± 2.8	10.6 ± 3.2
Spleen/Muscle	9.9 ± 3.0	17.3 ± 7.4	10.8 ± 2.7	4.7 ± 1.3
Stomach/Muscle	2.3 ± 1.0	1.1 ± 0.6	2.6 ± 0.9	0.9 ± 0.2
Small Int/Muscle	2.4 ± 0.8	1.5 ± 0.7	2.9 ± 0.2	0.6 ± 0.2
Large Int/Muscle	3.9 ± 1.4	3.2 ± 1.3	5.5 ± 1.1	1.4 ± 0.4
Kidneys /Muscle	13.7 ± 4.3	9.8 ± 4.0	15.4 ± 2.8	3.3 ± 0.8
Testes/Muscle	6.5 ± 2.3	4.8 ± 1.9	7.4 ± 1.6	1.9 ± 0.5
Bladder/Muscle	5.4 ± 1.8	4.7 ± 3.2	4.8 ± 1.0	1.8 ± 1.0
Anterior	1.1 ± 0.3	0.7 ± 0.4	1.3 ± 0.2	0.9 ± 0.6
D/V/L	7.2 ± 2.1	2.6 ± 1.0	1.3 ± 0.6	1.3 ± 0.3
Skin/Muscle	4.0 ± 1.5	2.8 ± 1.1	4.6 ± 0.7	0.4 ± 0.1
Pancreas/Muscle	2.1 ± 0.7	1.5 ± 0.9	2.0 ± 0.2	–
Brain/Muscle	0.3 ± 0.1	–	0.4 ± 0.03	0.1 ± 0.05
Tail/Muscle	5.1 ± 2.3	–	4.9 ± 0.5	0.6 ± 0.2
Muscle/Muscle	1.0 ± 0.4	1.0 ± 0.5	1.0 ± 0.1	0.3 ± 0.1
Bone/Muscle	7.4 ± 3.9	8.2 ± 3.1	7.1 ± 2.2	1.0 ± 0.3
Seminal	0.8 ± 0.4	0.4 ± 0.2	0.5 ± 0.1	0.6 ± 0.3
Fat/Muscle	0.7 ± 0.3	0.9 ± 0.4	1.0 ± 0.1	0.4 ± 0.1

[a] Data are expressed as the mean %ID/g ± one standard deviation (S.D.) [b] D/V/L = dorsal/ventral/lateral prostate lobes. [c] Errors on tissue-to-muscle ratios are calculated as the geometric mean of the standard deviations. Int = intestine. [d] See experimental section for details.

Supplementary Figure 18. Biodistribution of ^{89}Zr-mTf in Hi-Myc and WT mice

Bar chart showing biodistribution data (%ID/g) for the uptake of ^{89}Zr-mTf (11.6–13.7 MBq, [313–370 μCi], 35–41 μg of protein/mouse) in Hi-Myc (12 month and 4 month old), WT immunocompetent FVB mice, as well as a blocking study in Hi-Myc (12 mo; 200 mg/kg non-radiolabelled holo-Tf) at 24 h post-i.v. administration. Int = intestine; AP = anterior prostate lobes; D/V/L-P = dorsal/ventral/lateral prostate lobes; SV = seminal vesicles.

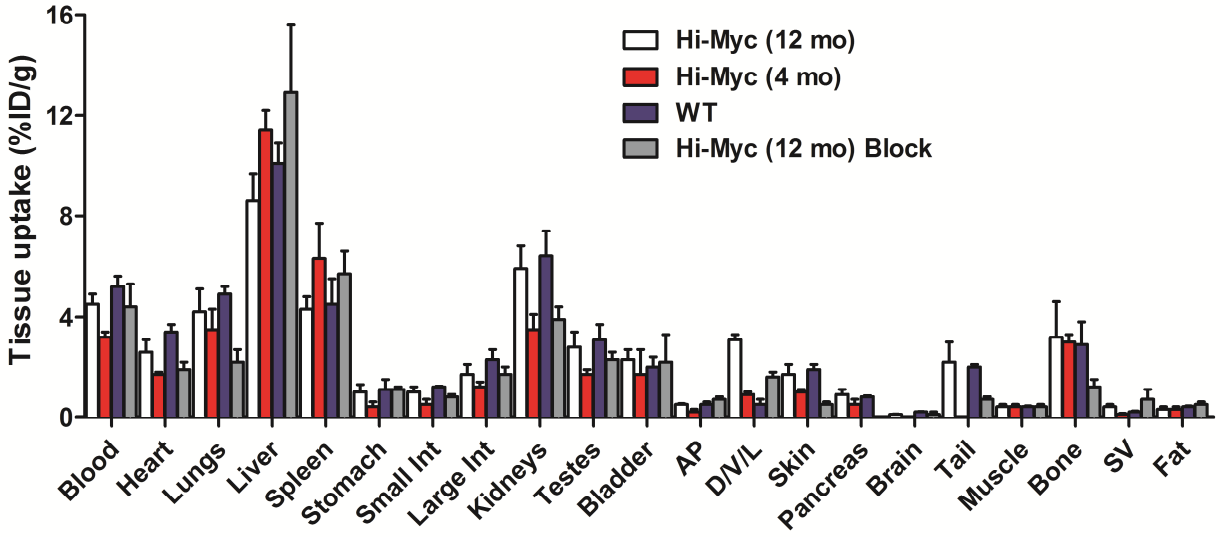

Supplementary Table 7. Student's *t*-test values for ^{89}Zr-mTf uptake in Hi-Myc (12 month) and WT mice based on biodistribution data

Tissue 1	Tissue 2	*P*-value [a]
Hi-Myc D/V/L-P	**Hi-Myc AP**	**0.00012**
Hi-Myc D/V/L-P	Hi-Myc bladder	0.06537
Hi-Myc D/V/L-P	Hi-Myc SV	<0.00001
Hi-Myc bladder	WT bladder	0.34800
Hi-Myc D/V/L-P	**WT D/V/L-P**	**0.00006**
Hi-Myc SV	WT SV	0.09301
Hi-Myc AP	WT AP	0.17668
Hi-Myc AP	WT bladder	0.01856
Hi-Myc AP	Hi-Myc SV	0.21803
Hi-Myc bladder	Hi-Myc AP	0.01654
Hi-Myc bladder	Hi-Myc SV	0.01085

[a] *P*-values < 0.05 are considered statistically significant differences.

Supplementary Figure 19. Blocking studies: ^{89}Zr-mTf PET imaging of Hi-Myc (12 month) animals

The specificity of ^{89}Zr-mTf uptake in the prostate tissue of Hi-Myc (12 mo) transgenic mice was demonstrated by *in vivo* and *ex vivo* PET imaging studies. (**a**) Representative coronal and sagittal PET images recorded *in vivo* at 24 h post-i.v. administration of ^{89}Zr-mTf (11.6–13.7 MBq, [313–370 µCi], 35–41 µg of protein/mouse). Mice were administered a blocking dose of non-radiolabelled holo-Tf (200 mg/kg) by i.v. tail vein injection at 45 min. before radiotracer administration. The presence of local prostatic adenocarcinoma was confirmed in all mice by MRI prior to commencing radiotracer studies. H = heart; L = liver; B = bladder; PCa = prostate adenocarcinoma. (**b**) *Ex vivo* PET image of the excised prostate from the mouse shown in Fig. S18a. SV=seminal vesicle; AP=anterior prostate; DP=dorsal prostate; LP=lateral prostate; VP=ventral prostate. In comparison to the radiotracer accumulation shown in non-blocked mice (Fig. 3a and b, main text), images and biodistribution data (Fig. 3g) confirm that focal uptake of ^{89}Zr-mTf in the prostate cancer of Hi-Myc (12 mo) is blockable, and hence, specific for the MYC-driven expression of TRFC.

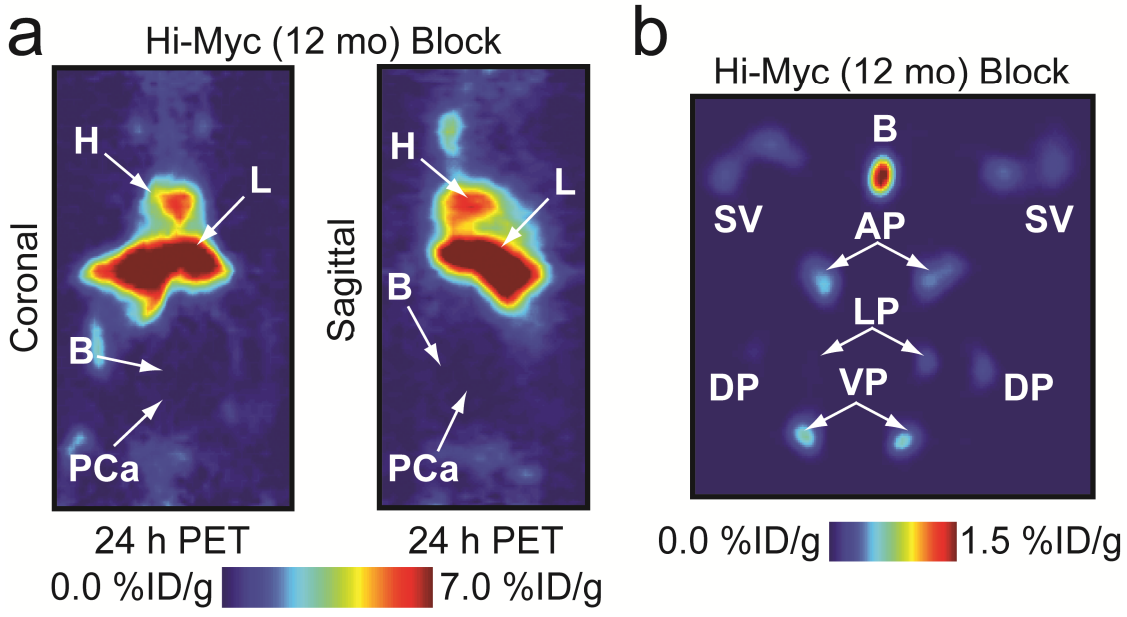

Supplementary Table 8. Quantitative VOI analysis from *ex vivo* prostate PET imaging

	Hi-Myc (12 mo)			Hi-Myc (4 mo)			WT			Hi-Myc (12 mo) Block		
Tissue	**Max. %ID/g**	**SD**	***n*** [a]	**Max. %ID/g**	**SD**	***n***	**Max. %ID/g**	**SD**	***n***	**Max. %ID/g**	**SD**	***N***
Measured tissue uptake from PET VOI analysis												
Bladder	1.74	0.09	4	0.36	0.08	5	1.46	0.12	8	2.29	0.30	5
SV	0.40	0.08	7	0.16	0.03	8	0.24	0.04	9	0.52	0.09	8
AP	0.81	0.17	5	0.07	0.01	4	0.18	0.04	6	0.65	0.13	8
DP	1.46	0.33	8	0.26	0.05	6	0.19	0.04	5	1.05	0.21	7
LP	1.23	0.28	8	0.15	0.03	4	0.09	0.02	4	1.22	0.25	7
VP	0.43	0.10	4	0.08	0.02	4	0.22	0.05	6	1.44	0.34	8
Tissue-to-bladder max. uptake ratios												
AP	0.57	0.08	5	0.21	0.03	4	0.13	0.04	6	0.28	0.13	8
DP	1.91	0.17	8	0.72	0.01	6	0.13	0.04	5	0.46	0.21	7
LP	1.61	0.33	8	0.43	0.05	4	0.06	0.04	4	0.53	0.25	7
VP	1.06	0.28	4	0.23	0.03	4	0.15	0.02	6	0.63	0.34	8
SV	0.53	0.10	7	0.46	0.02	8	0.17	0.05	9	0.23	0.09	8

[a] *n* = number of 2-deimensional regions-of-interest (ROI) used in the VOI analysis. These data correspond to the *ex vivo* PET images and quantification shown in **Figure 3** of the main text and **Supplementary Figure 19** (*vide supra*).

Supplementary Figure 20. Example of region-of-interest definitions used in quantitative PET analysis

The figure shows representative 2-dimensional regions-of-interest (ROIs) used to define 3-dimensional VOIs to measure the uptake of ^{89}Zr-mTf in various tissues based on PET imaging of Hi-Myc (12 mo) and WT mice. NB: ROIs are defined by the white margins. H = heart; L = liver; B = bladder; M = muscle; PCa = prostate adenocarcinoma.

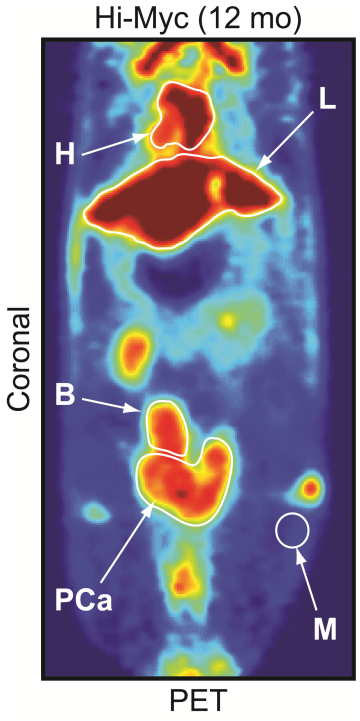

Supplementary Figure 21. Truth plot of mean PET tissue uptake (%ID g^{-1}) *versus* biodistribution (%ID g^{-1})

Analysis of the relationship between quantitative PET analysis and biodistribution studies in for ^{89}Zr-mTf uptake in the prostate, heart/blood pool, liver and muscle in normal and blocked Hi-Myc (12 mo), and WT mice at 24 h post-radiotracer administration. (**a**) Truth plot of the measured mean tissue uptake (%ID/g) from PET images *versus* uptake measured by *ex vivo* biodistribution studies on the same mice. As expected, a strong, positive linear relationship (R^2 = 0.97) can be observed whereby tissue uptake values measured from PET slightly underestimate the true values measured from the biodistribution studies. Underestimation is a consequence of well-established partial volume errors (PVEs) that tend to reduce signal intensity from image analysis. (**b**) Plot of the residuals from **Supplementary Figure 21a**.

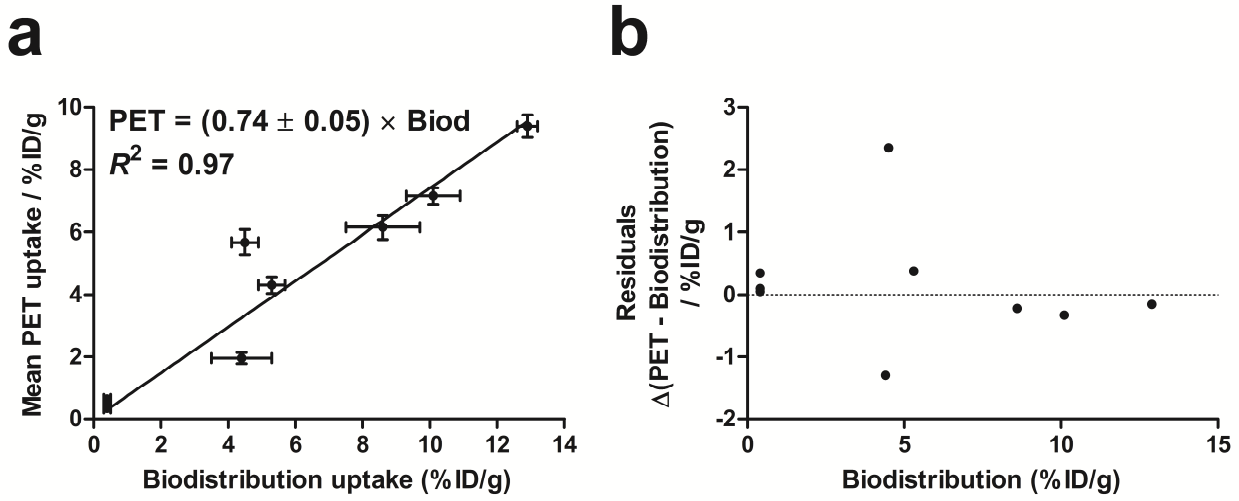

Supplementary Figure 22. Temporal PET studies of heat denatured ^{89}Zr-mTf in Hi-Myc (12 month) mice

The specificity of radiotracer uptake in the prostate tissue of Hi-Myc (12 mo) transgenic mice was also evaluated by investigating PET image data recorded using heat denatured ^{89}Zr-mTf.

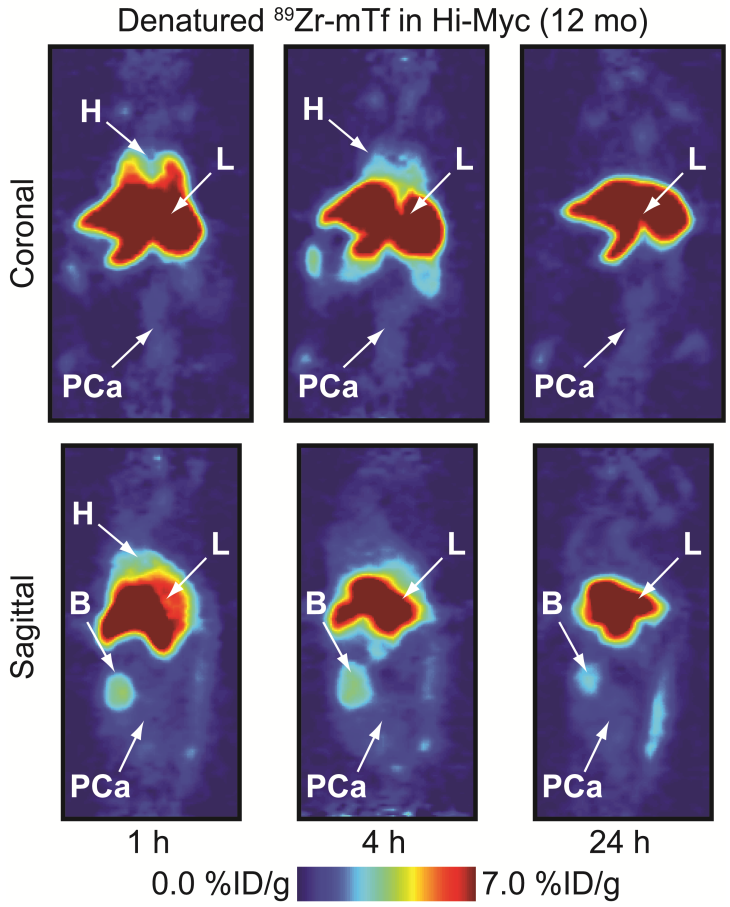

Formulated ^{89}Zr-mTf was heated for 10 min. at 80 °C to denature the Tf protein component. After cooling, ITLC and size-exclusion chromatography verified that the ^{89}Zr-radioactivity remained bound to the denatured Tf. The coronal and sagittal PET images, recorded at 1, 4 and 24 h post-radiotracer administration indicate that denatured ^{89}Zr-mTf is cleared rapidly from the blood pool with high accumulation of ^{89}Zr-radioactivity in the liver and no uptake found in the heart. In contrast to the studies described above for, no uptake of denatured ^{89}Zr-mTf was observed in the prostate tissue of Hi-Myc (12 mo) mice. Denatured ^{89}Zr-mTf showed slow clearance from the liver with no activity found in the abdominal region, minimal renal clearance, and low levels of ^{89}Zr-radioactivity accumulating in the bladder/urine.

References

1 Zanzonico, P. Routine quality control of clinical nuclear medicine instrumentation: a brief review. *J Nucl Med* **49**, 1114-1131 (2009).

2 Holland, J. P. *et al.* ^{89}Zr-DFO-J591 for immunoPET of prostate-specific membrane antigen expression *in vivo*. *J Nucl Med* **51**, 1293-1300 (2010).

3 MacGillivray, R. T. A. *et al.* Two High-Resolution Crystal Structures of the Recombinant N-Lobe of Human Transferrin Reveal a Structural Change Implicated in Iron Release. *Biochem* **37**, 7919-7928, (1998).

4 Holland, J. P., Sheh, Y. & Lewis, J. S. Standardized methods for the production of high specific-activity zirconium-89 *Nucl. Med. Biol.* **36**, 729-739, (2009).

5 Holland, J. P. *et al.* Measuring the pharmacokinetic effects of a novel Hsp90 inhibitor on HER2/*neu* expression in mice using ^{89}Zr-DFO-trastuzumab. *PLoS ONE* **5**, e8859 (2010).

6 Anderson, C. J. *et al.* Preparation, biodistribution and dosimetry of copper-64-labeled anti-colorectal carcinoma monoclonal antibody fragments 1A3-F(ab')$_2$. *J Nucl Med* **36**, 850-858 (1995).

7 Verel, I. *et al.* ^{89}Zr immuno-PET: Comprehensive Procedures for the production of ^{89}Zr-labeled monoclonal antibodies. *J Nucl Med* **44**, 1271-1281 (2003).

8 Watson, P. A. *et al.* Context-Dependent Hormone-Refractory Progression Revealed through Characterization of a Novel Murine Prostate Cancer Cell Line. *Cancer Res* **65**, 11565-11571, (2005).

9 Guide for the Care and Use of Laboratory Animals. Washington, DC: National Academy Press. (1996).

10 Ellwood-Yen, K. *et al.* Myc-driven murine prostate cancer shares molecular features with human prostate tumors. *Cancer Cell* **4**, 223-238 (2003).

11 Beattie, B. J. *et al.* Multimodality registration without a dedicated multimodality scanner. *Mol Imaging* **6**, 108-120 (2007).

12 Holland, J. P. & Lewis Jason, S. Zirconium-89 chemistry in the design of novel radiotracers for immuno-PET. *Technetium and Other Radiometals in Chemistry and Medicine, Eds: Ulderico Mazzi, William C. Eckelman, Wynn A. Volkert, Publisher: Servizi Grafici Editoriali snc, Padova, Italy*, 187-192 (2010).